NBS TECHNICAL NOTE 1034

U.S. DEPARTMENT OF COMMERCE / National Bureau of Standards

Backscatter Measurements on Optical Fibers

NATIONAL BUREAU OF STANDARDS

The National Bureau of Standards[1] was established by an act of Congress on March 3, 1901. The Bureau's overall goal is to strengthen and advance the Nation's science and technology and facilitate their effective application for public benefit. To this end, the Bureau conducts research and provides: (1) a basis for the Nation's physical measurement system, (2) scientific and technological services for industry and government, (3) a technical basis for equity in trade, and (4) technical services to promote public safety. The Bureau's technical work is performed by the National Measurement Laboratory, the National Engineering Laboratory, and the Institute for Computer Sciences and Technology.

THE NATIONAL MEASUREMENT LABORATORY provides the national system of physical and chemical and materials measurement; coordinates the system with measurement systems of other nations and furnishes essential services leading to accurate and uniform physical and chemical measurement throughout the Nation's scientific community, industry, and commerce; conducts materials research leading to improved methods of measurement, standards, and data on the properties of materials needed by industry, commerce, educational institutions, and Government; provides advisory and research services to other Government agencies; develops, produces, and distributes Standard Reference Materials; and provides calibration services. The Laboratory consists of the following centers:

Absolute Physical Quantities[2] — Radiation Research — Thermodynamics and Molecular Science — Analytical Chemistry — Materials Science.

THE NATIONAL ENGINEERING LABORATORY provides technology and technical services to the public and private sectors to address national needs and to solve national problems; conducts research in engineering and applied science in support of these efforts; builds and maintains competence in the necessary disciplines required to carry out this research and technical service; develops engineering data and measurement capabilities; provides engineering measurement traceability services; develops test methods and proposes engineering standards and code changes; develops and proposes new engineering practices; and develops and improves mechanisms to transfer results of its research to the ultimate user. The Laboratory consists of the following centers:

Applied Mathematics — Electronics and Electrical Engineering[2] — Mechanical Engineering and Process Technology[2] — Building Technology — Fire Research — Consumer Product Technology — Field Methods.

THE INSTITUTE FOR COMPUTER SCIENCES AND TECHNOLOGY conducts research and provides scientific and technical services to aid Federal agencies in the selection, acquisition, application, and use of computer technology to improve effectiveness and economy in Government operations in accordance with Public Law 89-306 (40 U.S.C. 759), relevant Executive Orders, and other directives; carries out this mission by managing the Federal Information Processing Standards Program, developing Federal ADP standards guidelines, and managing Federal participation in ADP voluntary standardization activities; provides scientific and technological advisory services and assistance to Federal agencies; and provides the technical foundation for computer-related policies of the Federal Government. The Institute consists of the following centers:

Programming Science and Technology — Computer Systems Engineering.

[1]Headquarters and Laboratories at Gaithersburg, MD, unless otherwise noted;
mailing address Washington, DC 20234.
[2]Some divisions within the center are located at Boulder, CO 80303.

Backscatter Measurements on Optical Fibers

B.L. Danielson

Electromagnetic Technology Division
National Engineering Laboratory
National Bureau of Standards
Boulder, Colorado 80303

U.S. DEPARTMENT OF COMMERCE, Malcolm Baldrige, Secretary

NATIONAL BUREAU OF STANDARDS, Ernest Ambler, Director

Issued February 1981

NATIONAL BUREAU OF STANDARDS TECHNICAL NOTE 1034

Nat. Bur. Stand. (U.S.), Tech. Note 1034, 52 pages (Feb. 1981)
CODEN: NBTNAE

U.S. GOVERNMENT PRINTING OFFICE
WASHINGTON 1981

For sale by the Superintendent of Documents, U.S. Government Printing Office, Washington, D.C. 20402

Price $3.25 (Add 25 percent additional for other than U.S. mailing)

CONTENTS

LIST OF TABLES

LIST OF FIGURES

Table 1. List of Symbols, Nomenclature and Units

Symbol	Nomenclature	Units
a	Sellmeier coefficient	
A	Absorption coefficient	m^{-1}
b	Sellmeier coefficient	um
B	Bandwidth	Hz
C	Velocity of light	ms^{-1}
$C(\lambda)$	Wavelength dependent absorption	m^{-1}
D	Rayleigh scattering coefficient	$m^{-1}\lambda^{+4}$
E	Wavelength independent loss	m^{-1}
F	Capture fraction	
i	Detector current	A
IVPO	Inside vapor phase oxidation	
K	Attenuation constant for NDF	
L	Fiber length	m
n	Index of refraction	
n_1	Index of refraction on fiber axis	
n_2	Index of refraction of fiber cladding	
N	Group index	
NA	Numerical aperture	
NDF	Neutral density filter	
OVPO	Outside vapor phase oxidation	
P	Degree of polarization	
R	Reflectivity	
SNIR	Signal-to-noise improvement ratio	
SNR	Signal-to-noise ratio	
t	Time	s
v_g	Group velocity	ms^{-1}
W	Pulse width	s
X	Parameter equal to $2\alpha_s L$	
α_a	Absorption loss coefficent	m^{-1}
α_n	Non-Rayleigh scattering loss coefficient	m^{-1}
α_s	Rayleigh scattering loss coefficient	m^{-1}
α_T	Total loss coefficient = $\alpha_a+\alpha_n+\alpha_s$	m^{-1}
Δ	Relative index difference $\Delta = (n_1^2-n_2^2)/2n_1^2$	
θ	Half vertex angle of fiber output radiation	
λ	Wavelength	um
Φ	Power	W

BACKSCATTER MEASUREMENTS ON OPTICAL FIBERS

B. L. Danielson

An optical time domain reflectometer (OTDR) and its components are described in detail. The system performance for this device is examined. Experimental methods are described for the measurement of several parameters of interest in the characterization of optical fibers using the OTDR. These parameters include scattering loss and capture fractions for unperturbed fibers. Experimental capture-fraction values are reported for several step and graded-index fibers and these results are compared with theoretical predictions. Rayleigh backscatter signatures are also presented for several fibers from different manufacturers. Fault signatures are shown for some intrinsic and extrinsic fiber perturbations.

KEY WORDS: Backscattering; capture fractions; fiber scattering; optical time domain reflectometry; Rayleigh scattering.

1. INTRODUCTION

The optical time domain reflectometer (OTDR) is an instrument that was developed in 1976 [1,2] which has proved to be very useful in testing optical fibers. It is similar in operation to the time domain reflectometer that has been used for many years to examine and locate irregularities and mismatches in cables. In the optical case, the inherent Rayleigh backscattering which occurs in the fiber material also provides a visualization of the attenuation and scattering properties of the waveguide as a function of length. Not only can the attenuation of the fiber be estimated, but anomalies may be located and characterized. An excellent review article by Rourke [3] contains much useful information on the OTDR system and its application to a number of optical fiber measurement problems.

If a rectangular optical pulse of width W and peak power Φ_0 is injected into a fiber, the time-dependent response of the backscatter power at the input end of the fiber $\Phi(t)$ can be shown to be [4]

$$\Phi(t) = 0.5\ \Phi_0 W v_g\ [\alpha_s F_s + \alpha_n F_n]\ \exp\ [-\alpha_T v_g t] \qquad (1\text{-}1)$$

where v_g is the group velocity, α_s the Rayleigh scattering attenuation coefficient, and F_s is the Rayleigh capture fraction, that is, the fraction of the scattered radiation which is trapped in the fiber and returned in the backward direction. The quantities α_n and F_n refer to the corresponding variables for non-Rayleigh type scattering processes. The total attenuation coefficient, α_T is the sum of the scattering coefficients, α_s and α_n, and the absorption coefficient representing the conversion of pulse energy into heat, α_a. Equation (1-1) applies to a uniform reciprocal fiber. In the more general case, both scattering and absorption coefficients as well as capture fractions may be a function of length.

In this report, we will document various experimental techniques for measuring the parameters which occur in eq (1-1). We will also present examples of the observed characteristic backscatter responses, $\Phi(t)$, for fibers which do not possess uniform properties. These backscatter "signatures" will be presented for fibers as received from the manufacturers as well as for fibers which have aberrations induced by external means. We will attempt to correlate observed signatures with changes in the physical properties of the perturbed fibers.

Values of scattering coefficients, capture fractions, and other parameters appearing in eq (1-1) can be useful in the identification, characterization and location of anomalies occuring in secure optical fiber communication systems. Also, this information may be helpful in OTDR design work, computer modeling and military fiber and cable specification.

2. DESCRIPTION OF THE OTDR

2.1 Data Acquisition System

Figure 2-1 shows a block diagram of the main elements of the OTDR system used to generate the data described in this report. The system was mounted on a bench top and no effort was made toward making the device compact or transportable for field use. The main components will be described separately below. Figure 2-2 illustrates the nature of the unprocessed oscilloscope display for a graded-index fiber which demonstrates a scattering anomaly. Figure 2-3 represents the corresponding display from the boxcar integrator, and figure 2-4 the boxcar output on a logarithmic scale.

2.2 Laser Diode Sources

For OTDR applications it is desirable to have optical sources capable of producing high peak radiance and high repetition rate with pulse durations in the general range of 5 to 100 ns. If backscatter responses are to be used to estimate loss at the communication wavelength of interest, then the source should also emit radiation at that wavelength. In the spectral region around 850 nm, a suitable pulsed source is the single heterojunction GaAlAs laser diode which is available from a number of manufacturers [5]. The diode used in the present experiments was a RCA type C30012 [6] which was rated at 4 W peak power at a 1 kHz repetition rate. With this source and 1:1 imaging optics it was possible to get a maximum of about 1 W peak power coupled into most fibers.

Many RCA GaAlAs laser diodes are partially polarized. This property can help reduce the coupling loss if a Glan-Thompson prism or polarizing beam splitter is used. It was found that the degree of polarization depends on the current drive level and also varies from diode to diode. A good sample can have about 80 percent of the output radiation polarized in one direction.

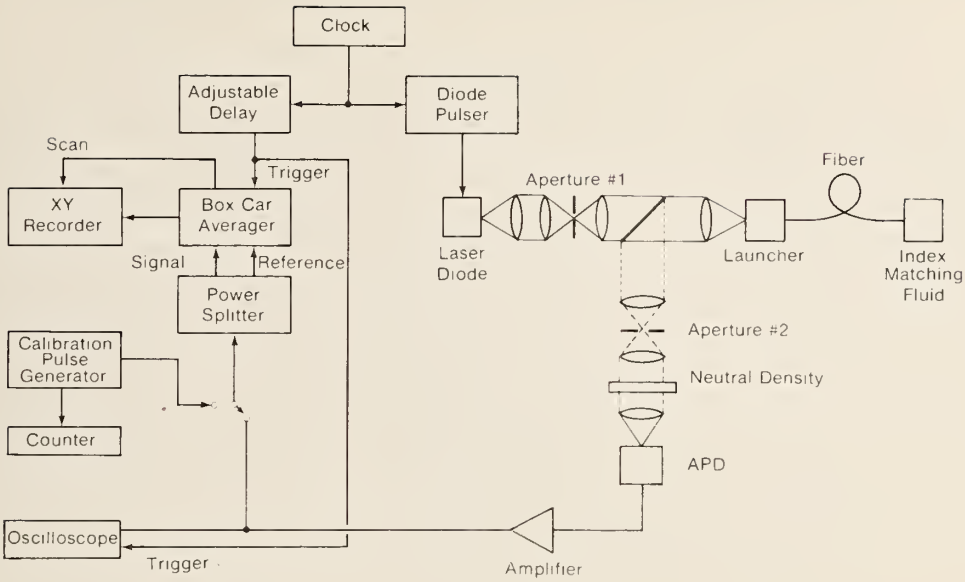

Figure 2-1. Block diagram of the OTDR system. All lenses are 10x microscope objectives.

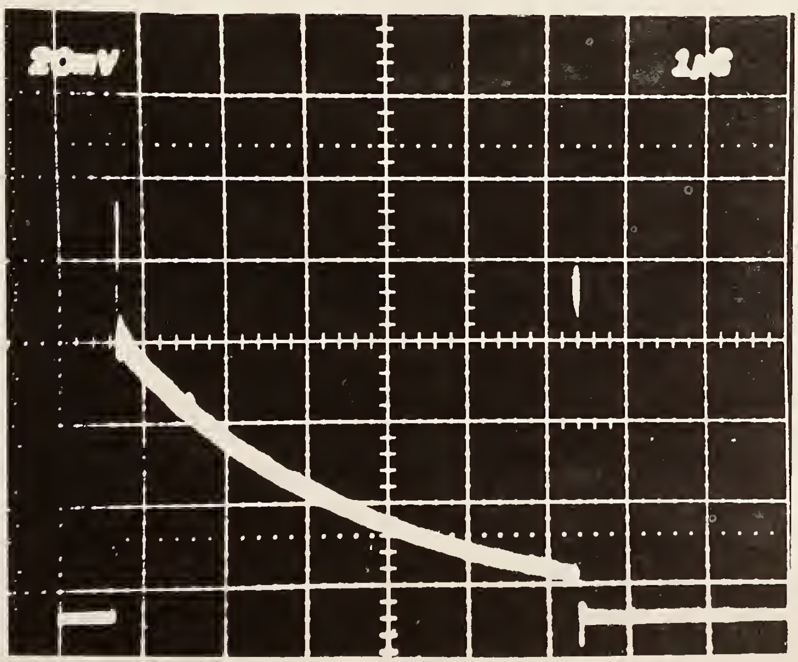

Figure 2-2. Backscatter signal, oscilloscope display. Fiber H.

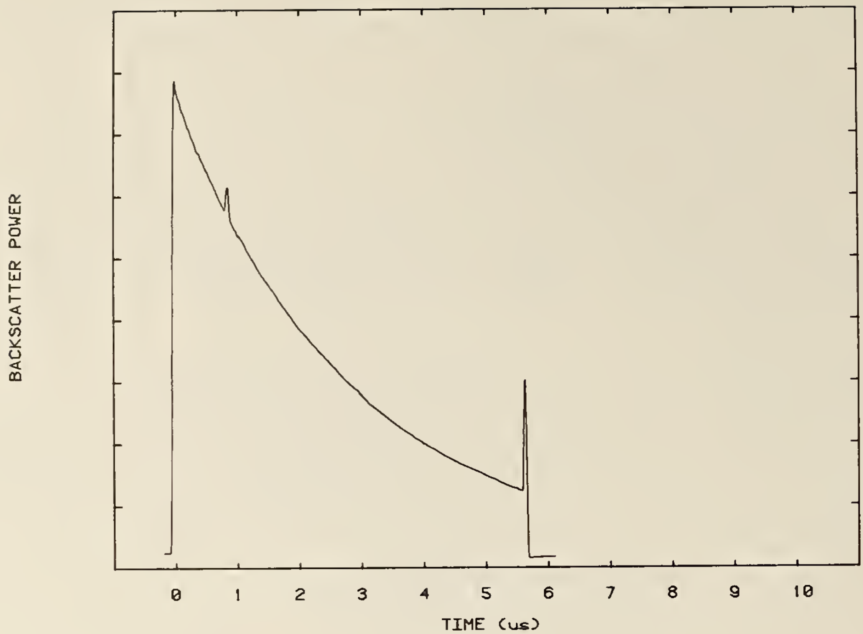

Figure 2-3. Backscatter signal, boxcar averager display. Fiber H.

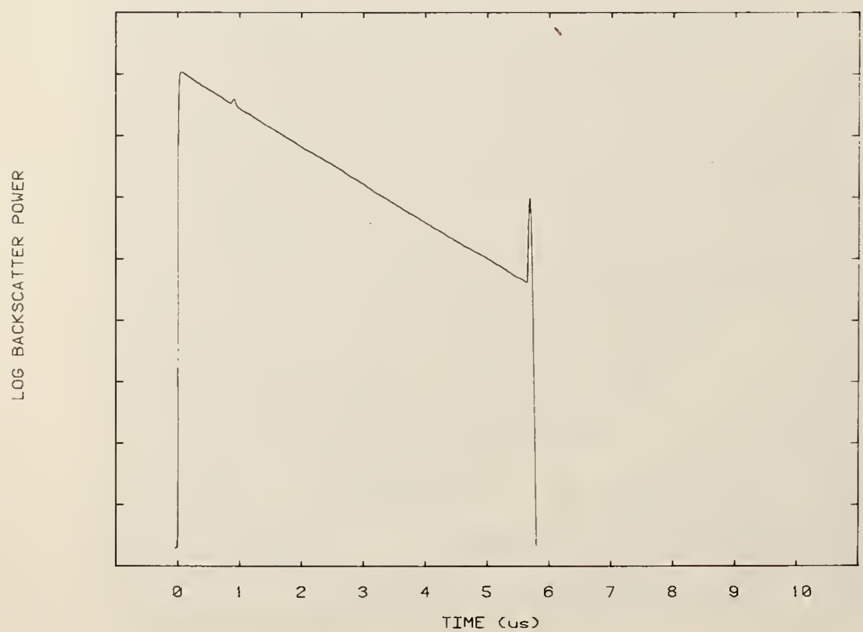

Figure 2-4. Backscatter signal, boxcar averager display, logarithmic scale. Fiber H.

Higher average output powers are possible with thermoelectric cooling of the laser diode [7]. No cooling devices were used in the present work, however.

2.3 Detectors

In view of the low signal levels involved in backscatter systems, the detector usually has internal gain. This can be either an avalanche photodiode (APD) or photomultiplier tube (PMT). In our somewhat limited experience with both of these types of detectors, we have found the APD to be preferable from several standpoints. In the present case we used an RCA type C30818E silicon APD [8]. For accurate measurements, the linearity of the detector at the normal operating gain is an important consideration. We checked the linearity in the following manner. A calibrated neutral density filter (NDF) with approximately 3 dB attenuation (neutral density 0.3) was inserted in the backscatter beam and the signal level noted. Comparison between the unattenuated and observed signal levels yields a quantitative measure of the detector linearity. When using this method, the NDF should always be inserted in the beam where the rays are parallel and allowance should be made for the fact that the focused beam may be displaced slightly. If the detector response is not uniform across its sensitive area, the apparent detector responsivity may change. This problem may to a large extent be obviated by mounting the detector on a XYZ translator and maximizing all signals prior to reading. Figure 2-1 shows an appropriate location for insertion of the NDF. Linearity may also be checked over a wider dynamic range with this method by using higher density filters.

2.4 Beamsplitters

Several types of possible OTDR beamsplitters and some of their characteristics are illustrated in figure 2-5. The coupling loss which is listed in the figure is based on the assumption that the backscattered radiation is unpolarized, since few fibers maintain polarization for more than a few meters [9]. The coupling loss is then defined as

$$\text{Coupling loss} = 10 \log \frac{\Phi_1}{\Phi_2} \text{ (dB)} \tag{2-1}$$

where Φ_1 is the collimated laser diode output power and Φ_2 is the power that is directed toward the detector after having undergone a lossless reflection. For polarizing beamsplitters this coupling loss will depend on the initial state and degree of source polarization. The minimum loss is for 100 percent polarization in the direction indicated by the arrows in figure 2-5.

Most commercially available 50:50 (nominal) beamsplitters do not have an exact 50:50 beamsplitter ratio, and this ratio may be a function of wavelength. Figure 2-6 demonstrates how the coupling loss changes with reflectivity (we assume that transmission + reflection = 1).

Figures 2-5(b) and 2-7 indicate that a fairly efficient beamsplitter can be constructed from a glass plate if it is used at a high angle of incidence. The parameter P represents

Beam Splitter Type	Coupling Loss	Remarks
(a) 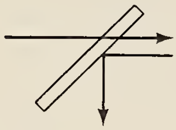	6 dB	One surface coated for 50% transmission. See figure 2-6.
(b) 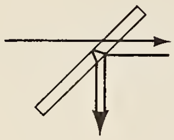	5 dB min.	Glass plate, n=1.51. See figure 2-7.
(c) 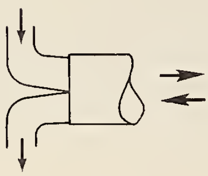	6 dB	Optical fiber coupler. See text.
(d) 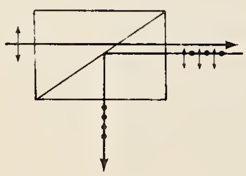	3 dB min.	Glan prism polarizer. Polarizer direction indicated by arrows.
(e) 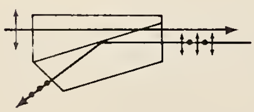	3 dB min.	Beam splitting Thompson prism.
(f) 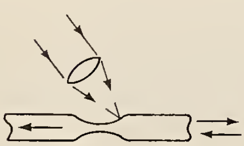		Taper coupler [1].

Figure 2-5. Types of OTDR beam splitters.

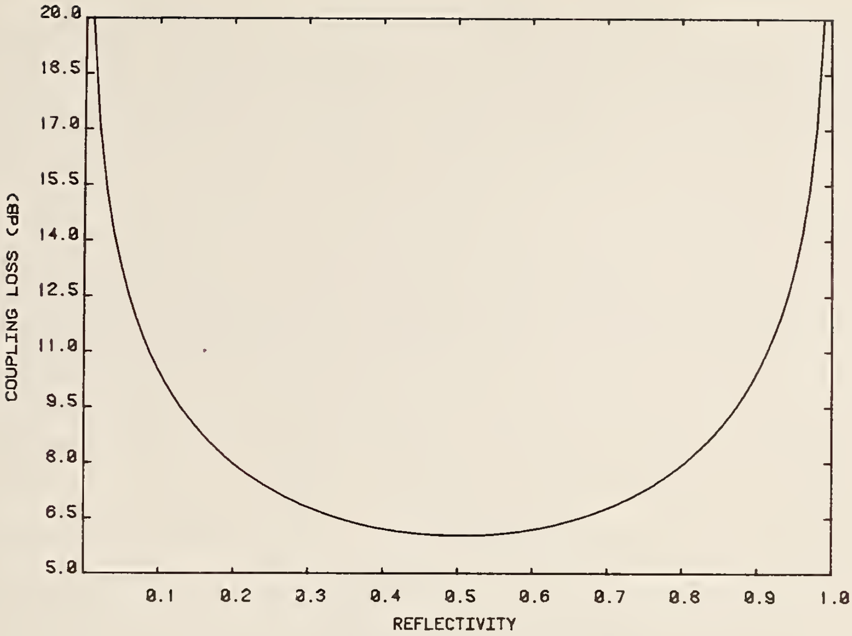

Figure 2-6. Coupling loss as a function of beam splitter reflectivity.

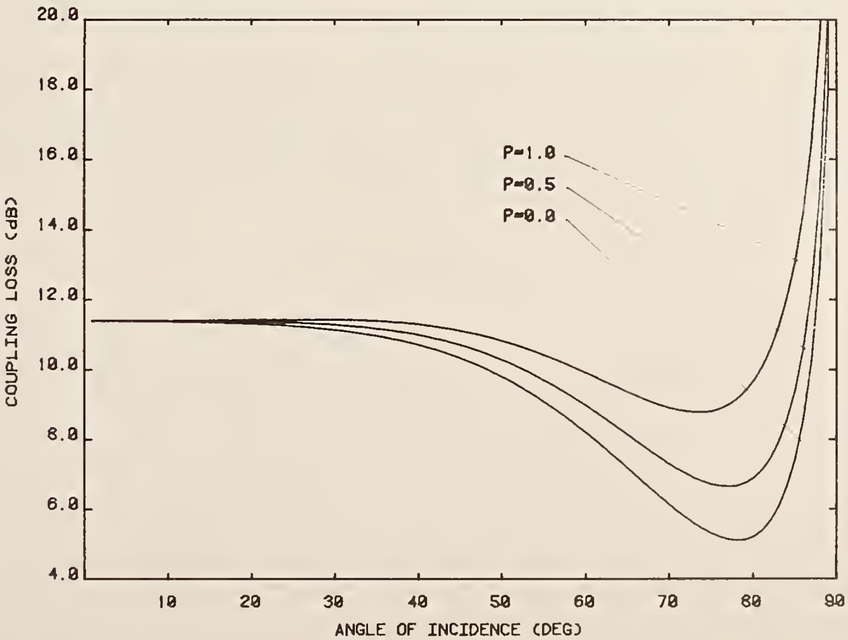

Figure 2-7. Coupling loss for a glass plate beam splitter as a function of angle of incidence for different degrees of polarization of the incident beam.

the fraction of the laser diode power which is polarized in the direction perpendicular to the plane defined by the normal to the plate surface and the incoming beam propagation vector. In the calculation of the coupling loss for this device we have taken into account reflections from both the front and back surfaces. The Fresnel equations [10] were used to determine the reflectivity as a function of angle of incidence. A prism may also be used in the same manner.

If space is a consideration, the beam splitter illustrated in figure 2-5(c) is another possibility. The laser diode, detector and test fiber can be connected together by appropriate pigtails. Since numerical apertures of fibers are independent of their diameters, the diode can couple into the launch fiber with a relatively high efficiency in the forward direction. The coupling loss is calculated from branching ratios determined from the relative fiber cross sections presented to the backward traveling wave. This arrangement apparently has not been described in the literature.

We have employed the Glan prism of figure 2-5(d) in the current work. This beam splitter provides good isolation (-37 dB) to Fresnel reflections from the input end of the fiber, and has a relatively low coupling loss. One disadvantage is the fact that the prism material is dispersive; the backscattered radiation is returned at different angles as the wavelength is changed. Use of different laser sources causes misalignment at the detector. The Foster or beam-splitting Glan-Thompson prism shown in figure 2-5(e) corrects this problem, but at considerable expense. Polarizing beam splitters do not have this difficulty, but the thin films that comprise the beam splitting surface do not maintain their polarizing properties over a wide spectral interval.

The taper coupler (fig. 2-5(f)) has been described by Barnoski et al. [1].

Other types of beam splitters have been described in the literature, including bifurcated couplers [11], and a patented coupling cell filled with index-matching liquid and a beam splitter [12]. Optical fiber directional couplers are also available commercially, but have not been evaluated by our laboratories.

2.5 Boxcar Averager

The signal averaging device used in the present work was a PAR Model 162 boxcar integrator. This particular instrument has the desirable feature that ratios may be taken of the scanned backscatter signal and an unscanned reference signal. The latter is obtained from a power divider after the first stage of amplification. This type of signal processing minimizes the effect of drift in the laser diode source and detector.

The adjustable delay (fig. 2-1) allows the boxcar scan to begin at any desired point in time. Since time maps into distance along the fiber, this is equivalent to starting the scan at any desired fiber location.

The time scan of the boxcar averager may be calibrated with markers which are output from a pulse generator. Time intervals are measured with an electronic timer/counter. The display time for a full scale scan is then accurate to within an estimated 0.02 percent.

2.6 Launcher

A fiber launcher which we have found to be convenient is shown in figure 2-8. This is an adaptation of a device originally described by Dakin et al. [13]. It consists of a precision-bore capillary tube [14] which is flared at one end for easy insertion of the fiber. The usual capillary diameter of 0.152 mm will hold 0.125 mm o.d. fibers without creep once the fibers are inserted. The launcher is filled with index-matching oil which also serves as a mode stripper. Once aligned, fibers may be removed and reinserted without significant realignment. However, care must be exercised that dust or foreign matter does not contaminate the bore or launch end. The launcher is demountable so that it can be cleaned if desired.

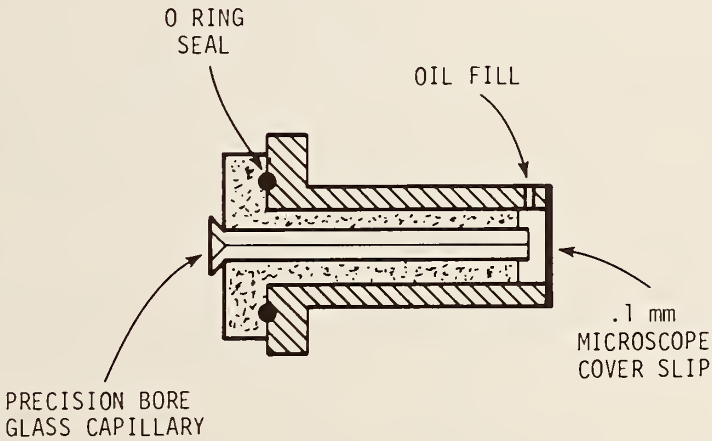

Figure 2-8. Demountable fiber launcher.

It is not necessary to use antireflection coatings on the glass cover slip on the input end if polarizing optics are used for the beam splitter. The reflection off the front surface is polarized and therefore largely rejected at the Glan prism coupler.

2.7 Apertures

The aperture labeled No. 1 in figure 2-1 is a laser-drilled pinhole and is used to control the spot size on the fiber. In certain cases, for example, with concentric-core fibers, it may be desirable to restrict the set of excited modes which are launched at the input end of the fiber. Alignment is facilitated if the optics have a magnification of one. Here the desired spot size is the same as the pinhole size and is independent of the launch NA. The aperture labeled No. 2 in the same figure is used to reduce the magnitude of the Fresnel reflection from the input end of the fiber. However, in many of the measurements reported on here, both apertures were removed in order to maximize the backscatter signal.

3. SIGNAL AND NOISE CONSIDERATIONS

3.1 Loss Budget

The ultimate limitation on the OTDR system for obtaining useful information from optical fibers will be associated with the problem of extracting useful signals in the presence of noise. The backscatter power levels are inherently small, and for fibers that are many kilometers in length, the signal-to-noise ratio (SNR) of the returning signal may be degraded to an unacceptable level. We will present here a numerical example of the backscatter signal levels to be expected in a somewhat idealized OTDR system for a special case. We consider a pure silica fiber whose only loss is due to the intrinsic Rayleigh scattering, and a laser diode whose radiation is 100 percent polarized. Other conditions are assumed as follows:

Pulse duration W	50 ns
Electronic bandwidth B	20 MHz
Rayleigh scattering loss (850 nm)	1.5 dB/km (3.45×10^{-4} nepers/m)
Absorption loss α_a	0 dB/km
Peak power input to fiber Φ_0	1 W (+30 dBm)
Beamsplitter coupling loss	6 dB
Optical losses (lenses, etc.)	0.2 dB
Group velocity v_g	2.01×10^8 m/s
Capture fraction F_s	0.005

From eq (1-1) we can calculate the maximum backscatter power in the fiber, at t=0, to be about -20.6 dBm, or considering the beamsplitter cooling loss and optical loss, a power of about -26.8 dBm at the detector. From design data presented elsewhere [15], we can infer that, for a given SNR, a typical APD requires a power level Φ_r of approximately

$$\phi_r = 10 \log B - 73 + [SNR-10]\ 0.88\ W. \qquad (3-1)$$

For a minimum SNR of 0 dB, we have

$$\Phi_r \cong -69 \text{ dBm} . \qquad (3-2)$$

This implies a loss margin of about 42 dB, so that a fiber may have a one way loss of 21 dB and still have an observable backscatter feature. For the silica fiber considered here this represents a length of about 14 km. In most cases the loss of commercially available fibers is much greaer than 1.5 dB/km at 850 nm so that the critical length is reduced correspondingly.

Figure 3-1 illustrates the backscatter signal levels expected from eq (1) as a function of fiber length for several probe pulse widths (at constant peak power) for silica at 850 nm. We have converted time to length according to the usual prescription $2L=tv_g$.

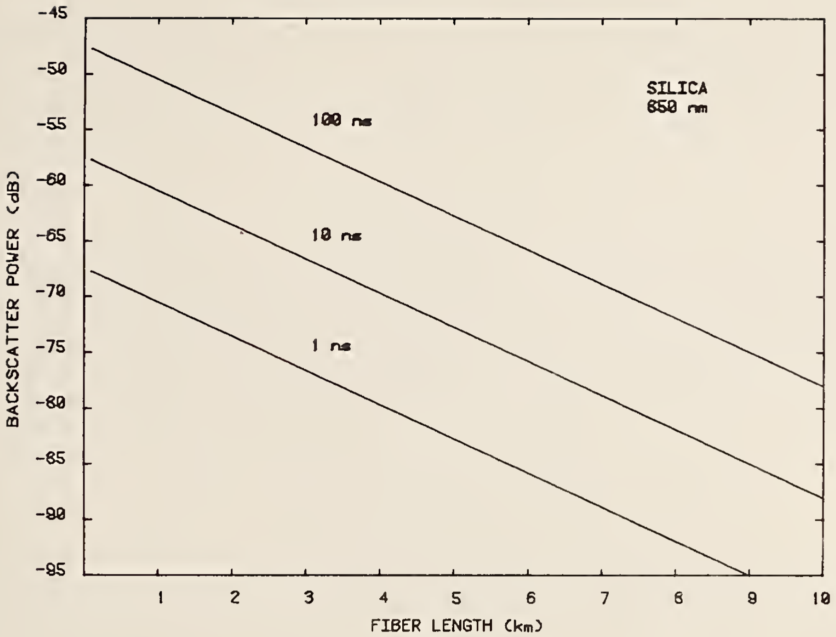

Figure 3-1. Backscatter power levels for silica at 850 nm. To a first approximation this power is proportional to the probe duration as shown here. Other conditions are given in the text.

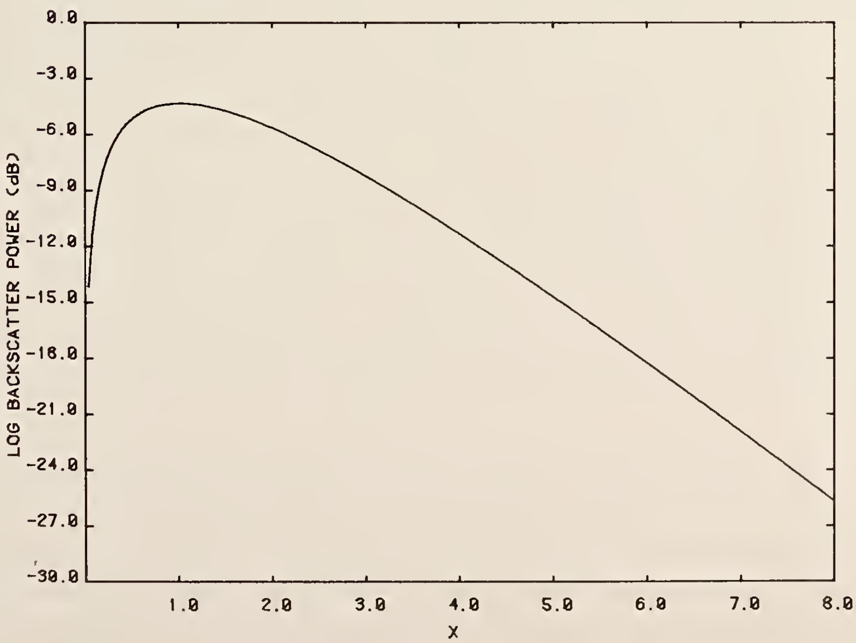

Figure 3-2. Relative backscatter power as a function of the parameter X (see text).

3.2 Optimum Scattering Levels

An examination of eq (1-1) shows that the backscatter power is proportional to the Rayleigh scattering loss α_s. Being a form of loss, α_s also decreases the signal as a funtion of length through the exponential factor $\exp(-\alpha_T v_g t)$. For a given length, L, then, there is an optimum α_s which maximizes the backscatter signal at that point. This is easily seen to be

$$\alpha_s = \frac{1}{2L} . \tag{3-3}$$

where α_s has units of nepers/m and L is in meters. Figure 3-2 shows the relative backscatter signal as a function of the parameter $X=2\alpha_s L$. We have normalized this plot in such a way that $0.5\ FWv_g = 1$. As an example, for a fiber length of 2.6 km, the maximum backscatter signal occurs for a Rayleigh scattering loss which is just equal to that of pure silica (850 nm).

3.3 Signal-to-Noise Ratio Improvement

There are many possible avenues for improving the SNR of the backscatter signal. For example, one can increase the averaging time, peak power, or increase the pulse width at quasi-constant power. However, these strategies often have their limits, and sometimes have deleterious side effects. We will now examine some of these possibilities.

Increasing the peak power, for example with a YAG laser, can result in nonlinear scattering processes, although for multimode fibers the thresholds appear to be very high [16, 17]. Often high peak powers are simply not available at the wavelength of interest.

With many laser diode sources it is possible to increase the pulse width at constant peak power output, without exceeding the maximum drive current specifications. The optical backscatter power is directly proportional to the probe pulse width W according to eq (1-1). For square-law detectors the corresponding electrical power is proportional to the square of the optical power. Also, in this case, the electronic signal bandwidth can be adjusted to be approximately 1/W (Hz); for white noise the (electrical) noise power will be inversely proportional to pulse width. We then have an apparent signal-to-noise improvement which varies as the third power of the pulse width W. However, fault-location resolution is degraded as a consequence. In addition, if $W > 1/\alpha_T v_g$, the background backscatter signature is distorted, making attenuation measurements less accurate and interpretation of anomalies more difficult.

It is well known that the SNR also can be increased by appropriate averaging. For Gaussian noise processes, averaging N samples will reduce the mean rms current noise by a factor of $N^{-1/2}$, or the mean noise power by a factor of 1/N. One would expect then, that the SNR should increase directly with N or with averaging time. The boxcar integrator operates on this principle. However, these expectations are realized only for certain stationary random noise processes. In real-world systems, flicker noise, drifts, or nonrandom (coherent) types of interference will generally set a limit to the SNR which can be attained with an increase in averaging time.

4. MEASUREMENTS WITH UNPERTURBED FIBERS

4.1 Fiber Backscatter Signatures

An estimate of the total attenuation of an optical fiber is easily made from an examination of the background backscatter signature, that is the backscatter power versus time profile which is a characteristic of the fiber in question. As used here, the background signature refers to the response due to uniform Rayleigh scattering in the fiber and is distinguished from fault signatures discussed in a later section which arise from fiber irregularities or faults. The degree of agreement between backscatter-derived loss determinations and the conventional cut-back loss values depends on measurement procedures as well as the intrinsic properties of the fiber. The procedures and conditions necessary for good agreement have been discussed at length elsewhere [18]; we will note here only that if the properties of the fiber are uniform (not a function of length) and reciprocal (the same in both forward and backward directions) then the losses determined from the cut-back and backscatter methods sould be equal. In some cases the actual fiber attenuation may be inferred from OTDR measurements when these conditions are not fulfilled [19].

We will show in this section some typical backscatter scans, from which attenuation may be inferred, in order to demonstrate their appearance, the variability between manufacturers, and some possible significance to the fine structure which is often observed. It will sometimes be convenient to display the linear backscatter signature (fig. 4-1) and at other times the logarithmic signature (fig. 4-2). The linear display emphasizes irregularities near the launch end of the fiber and can be used to determine attenuation with no Y-axis calibration. The logarithmic display requires a system calculation to calibrate the Y-axis, but has a wider dynamic range and provides for easy visual identification of nonlinear loss regions. These are manifested by changes in slope.

Figures 4-1 to 4-3 represent the backscatter scans from a concentric-core fiber [20]. This type of fiber has a special geometry consisting of two step-type channels in one fiber. One of the cores is on axis and the second is in the form of a concentric annulus. It will be noted that there is a high degree of correlation in the irregularities appearing on the scans of both channels. These fluctuations are reproducible and are observed on most of the fibers we have tested. They are most likely due to diameter changes which arise while the fiber is being drawn. Rourke [3] has shown that diameter variations will produce effects of this sort, although other explanations have also been offered [21].

Figures 4-4 to 4-12 show the signatures of other fibers which also exhibit irregularities. In all of these samples, the fluctuations are a real effect and are not due to system noise. It is apparent that some fibers manifest much smaller variations than others. Fibers A and E (both from the same manufacturer) are particularly smooth in this regard. It is also clear that, for certain applications, such as secure communications, where it is desired to detect as small a fault signature as possible, these background irregularities should be minimized.

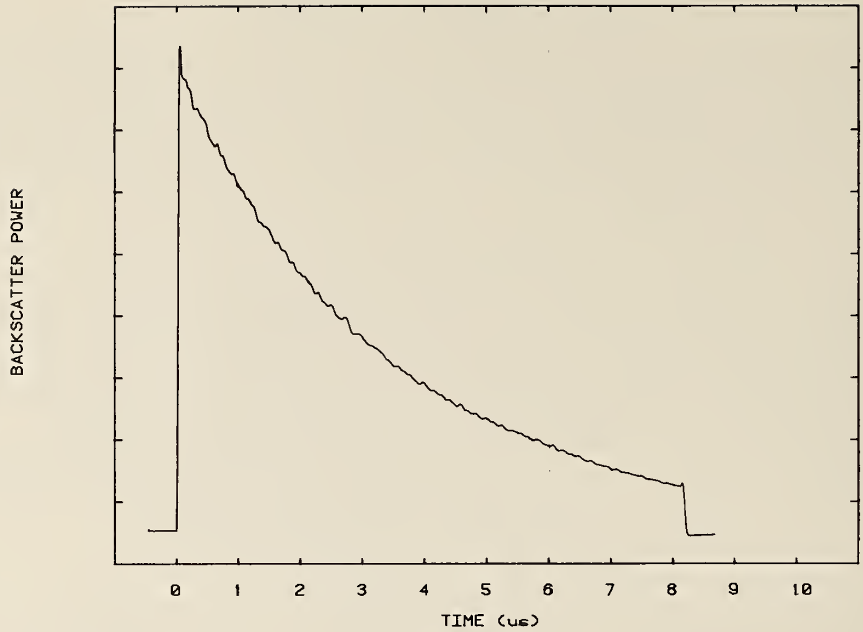

Figure 4-1. Backscatter response for a concentric-core fiber, center core. Fiber G.

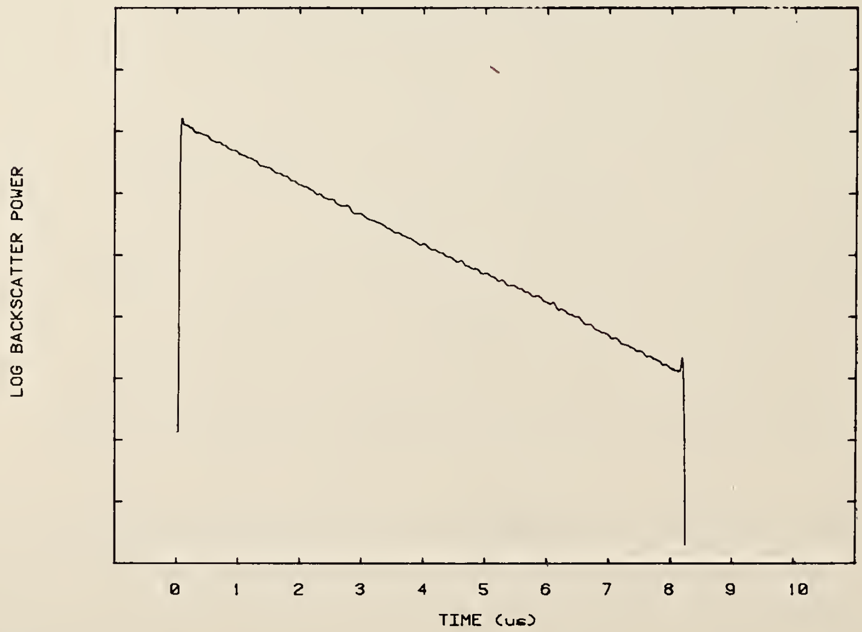

Figure 4-2. Backscatter response for a concentric-core fiber, center core, logarithmic scale. Fiber G.

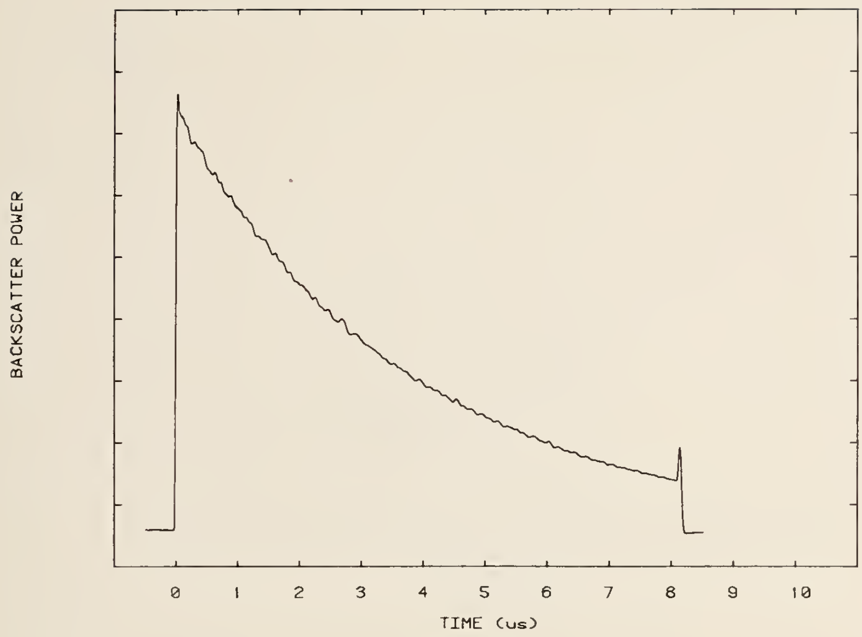

Figure 4-3. Backscatter response for a concentric-core fiber, outer core. Fiber G.

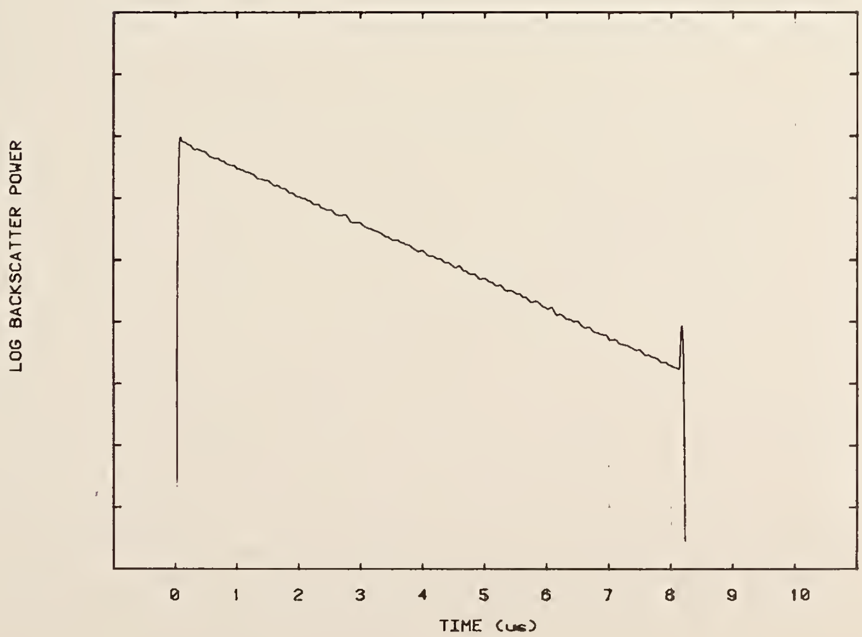

Figure 4-4. Backscatter response for a concentric-core fiber, outer core, logarithmic scale. Fiber G.

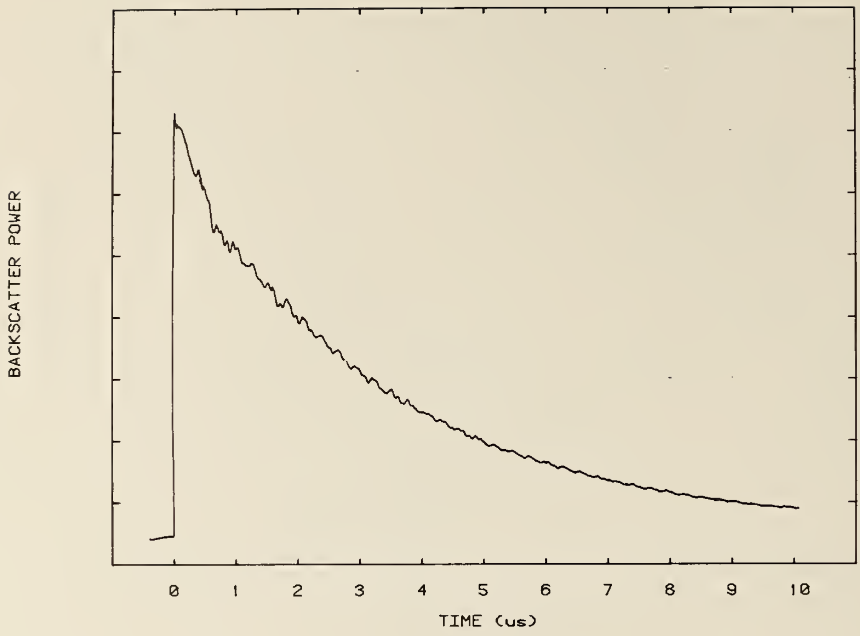

Figure 4-5. Backscatter response for step-index fiber F.

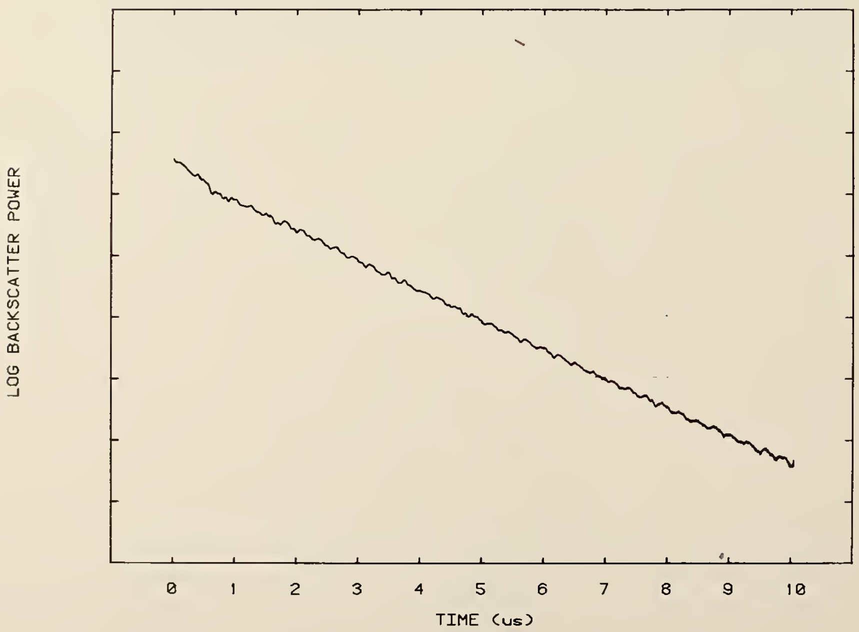

Figure 4-6. Backscatter response for step-index fiber F, logarithmic scale.

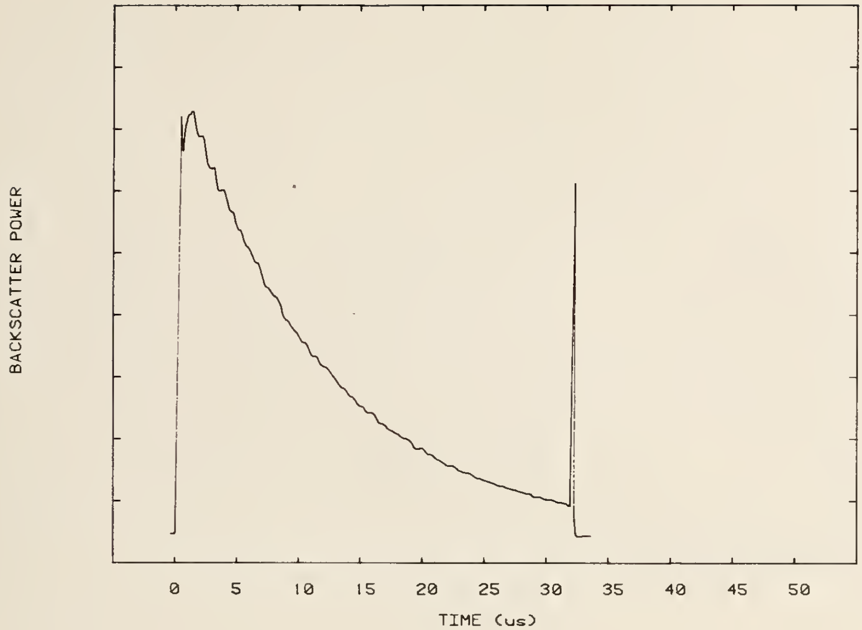

Figure 4-8. Backscatter response for graded-index fiber I, logarithmic scale.

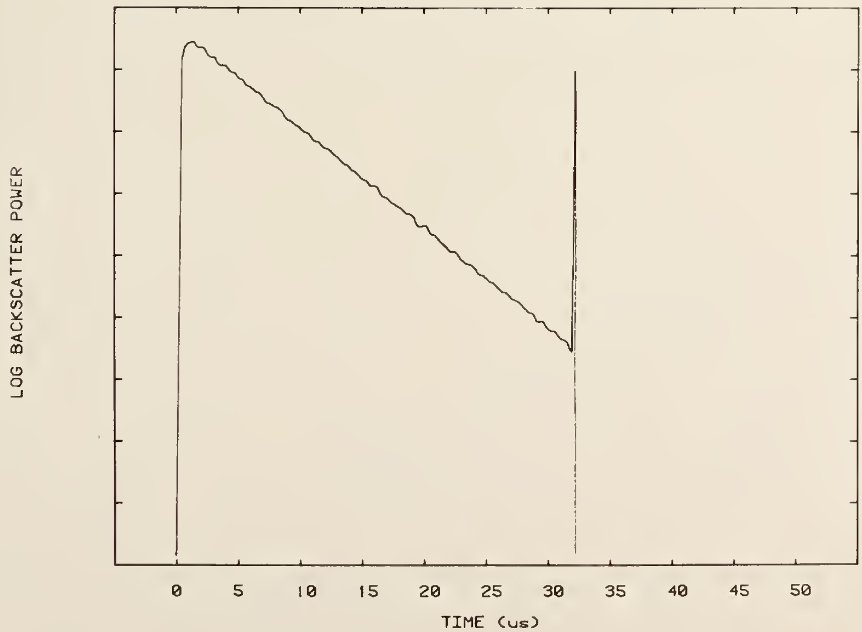

Figure 4-7. Backscatter response for graded-index fiber I.

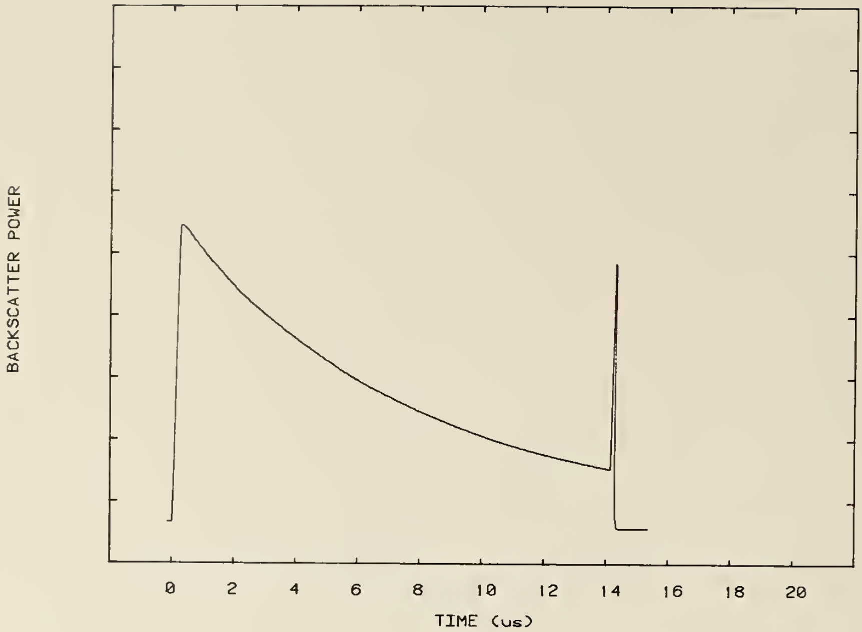

Figure 4-9. Backscatter response for graded-index fiber A.

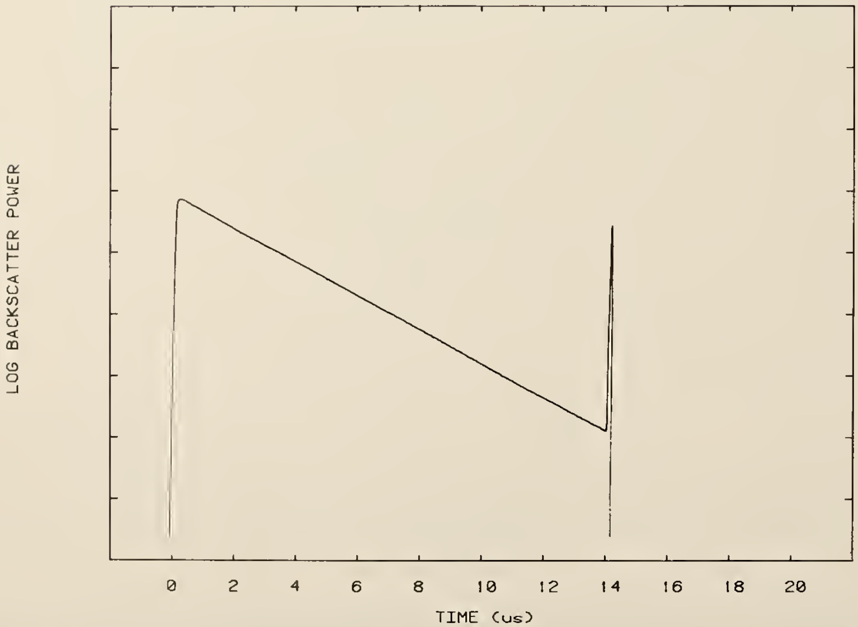

Figure 4-10. Backscatter response for graded-index fiber A, logarithmic scale.

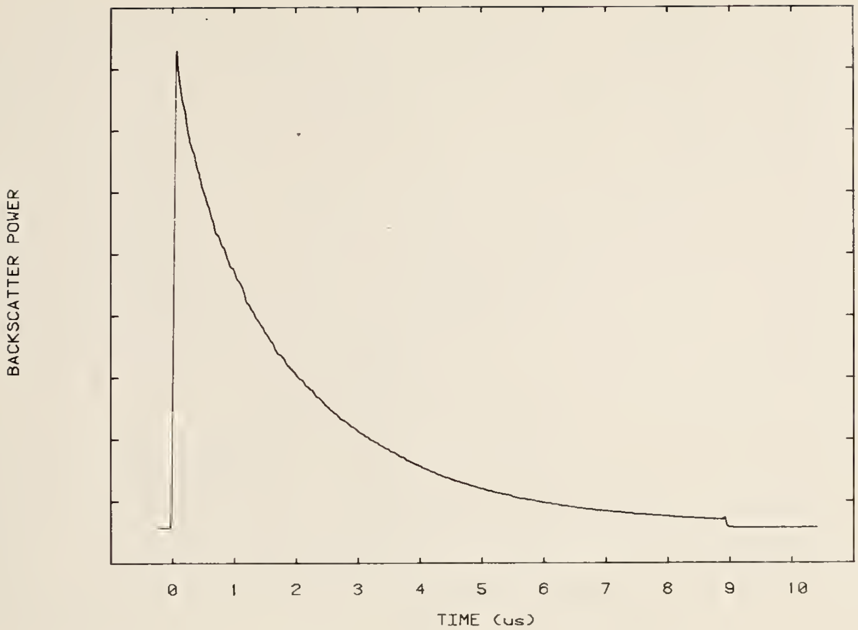

Figure 4-11. Backscatter response for graded-index fiber D.

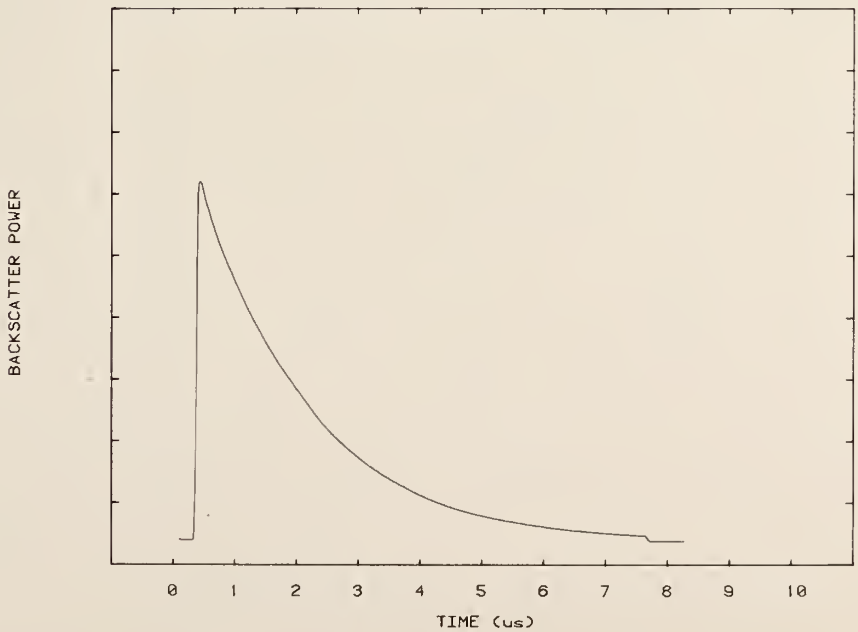

Figure 4-12. Backscatter response for step-index fiber E.

4.2 Scattering Loss Measurements

In eq (1-1) we have divided the scattering mechanisms in fibers into two different categories, Rayleigh and non-Rayleigh. Rayleigh scattering originates in intrinsic spatial variations in the index of refraction and in fluctuations in the dopant material which occur on a small scale compared with the wavelength. It is characterized by a $(1+\cos\theta)$ angular dependence and is inversely proportional to the fourth power of the wavelength. Olshansky [22] gives an excellent review of Rayleigh scattering in fibers, along with many useful references. Non-Rayleigh scattering includes such processes as microbending, core-cladding interface scattering, Mie scattering, radiation from bends (macrobending), and scattering, or reflection, from fiber imperfections. Most of these mechanisms will scatter radiation predominantly in the forward direction (i.e., F_n is small) so that their effects on the backscatter signature is similar to an absorption process.

Many different methods have been developed for measuring scattering in fibers [23,24, 25]. These are all variants of integrating spheres which have the severe disadvantage, in our application, of measuring forward as well as Rayleigh-type scattering. A technique proposed by Inada [26], and implemented by other authors [27,28], avoids this problem. In this method the spectral loss is plotted as a function of λ^{-4}. If α_T represents the total loss

$$\alpha_T = \frac{D}{\lambda^4} + E + C(\lambda) \tag{4-1}$$

where D is the Rayleigh scattering coefficient in units of $m^{-1}\ \lambda^{+4}$, E is the loss contribution which is independent of wavelength, and $C(\lambda)$ is the wavelength contribution which in our case is dominated by OH absorption. The Rayleigh scattering coefficient can be determined by a least-squares fit to eq (4-1) by ignoring wavelengths around 950 nm where water absorption is important. The fibers described in section 4.3.5 were measured in this fashion in order to obtain α_s values for capture fraction determinations. Some sample plots are shown in figures 4-13, 4-14, and 4-15 which show the variability of these types of plots. All are graded-index fibers. Fiber A demonstrates a loss dependence on launch NA. However, the Rayleigh scattering coefficient (the slope of the straight-line fit) is independent of launch NA. The difference in total loss has been attributed to excess core-cladding scattering [26]. Fibers B and D do not exhibit this effect. Fiber D has a very small residual loss coefficient E which was unusual in the fibers tested. It is instructive to compare these results with pure silica. Values of scattering coefficients vary somewhat depending on sample preparation and whether measurements are made on bulk material or fibers. Values of 0.80 dB $km^{-1}\ um^{+4}$ (1.84×10^{-4} nepers $m^{-1}\ um^{+4}$) are typical [29,30]. The lowest reported loss in a graded-index multimode fiber had a Rayleigh scattering coefficient of 1.0 dB km^{-1} um^{+4} [28]. Scattering levels usually increase with dopant concentration.

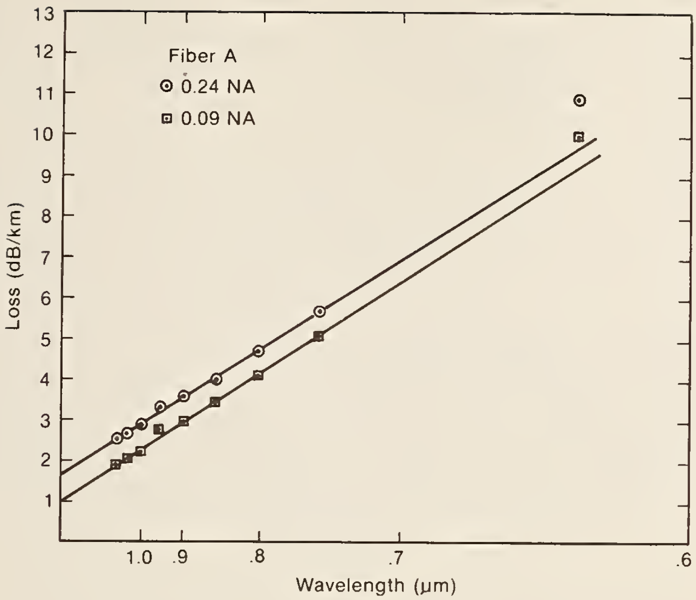

Figure 4-13. Measured loss spectra, fiber A.

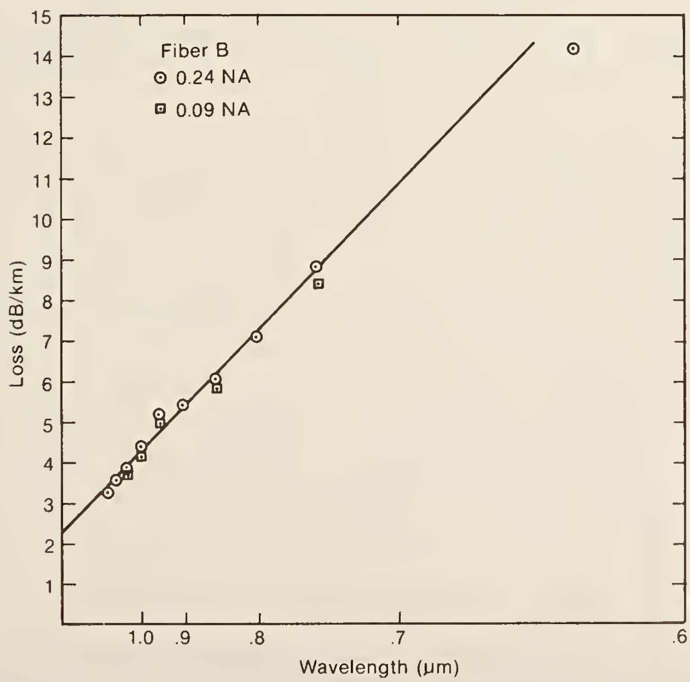

Figure 4-14. Measured loss spectra, fiber B.

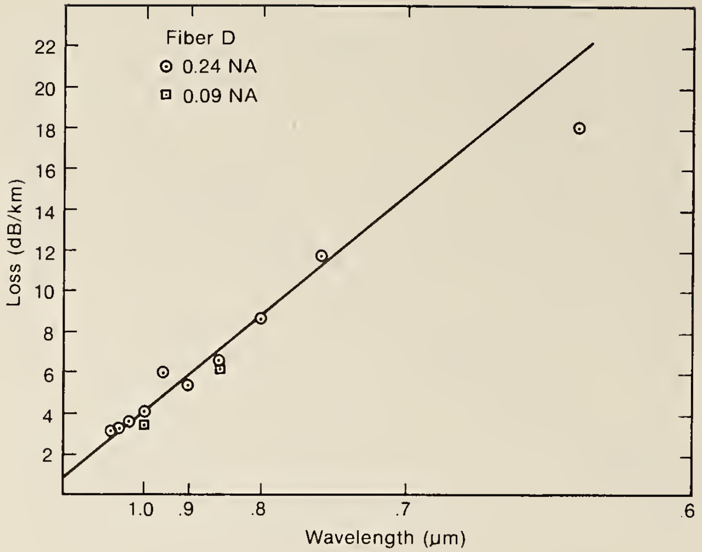

Figure 4-15. Measured loss spectra, fiber D.

4.3 Capture Fraction Measurements

4.3.1 Significance of Capture Fractions

The numerical value of optical fiber capture fractions contribute to the data base which is essential to design engineers in the following applications areas:

1. Passive (optical fiber) gyroscopes. The ultimate attainable SNR and accuracy will be dependent on backscatter power levels which are proportional to the capture fractions [31].
2. Full-duplex communication systems. In systems which employ a single wavelength for bidirectional transmission on a fiber, backscatter levels will determine the SNR and crosstalk [32,33].
3. OTDR systems. Backscatter signal levels will determine the allowable fiber loss for location of breaks or defects.
4. Computer simulation studies. Realistic values for F are required for proper computer modeling as described in section 6.

4.3.2 Theory and Experimental Methods

The capture fraction F (also referred to as the backscatter factor or trapping factor) represents the fraction of the radiation which is scattered or otherwise removed from the forward propagating pulse which falls within the acceptance cone of the fiber and is therefore confined within the guided wave structure. We will be concerned here only with that radiation travelling in a direction opposite to the probe pulse. The concept of capture fractions is usually restricted to Rayleigh scattering, but we will use it here in a broader sense; every process or event, discrete or distributed, which removes radiation from the probe pulse and returns at least some of this radiation in the back direction has associated with it a capture fraction. Table 2 lists the capture fractions which can be identified with some scattering and reflection processes in several different types of fibers. We have also included F values of some fiber perturbations which have their characteristic capture fractions. Some of these, as we will see in section 5, are too small to be measured but upper limits can be placed on their magnitude.

We will in the first instance concern ourselves with the actual experimental determination of fiber capture fractions associated with scattering processes which vary inversely with the fourth power of the wavelength: Rayleigh and Brillouin scattering. Brillouin scattering is expected to have the same angular and wavelength dependence as the Rayleigh scattering and will therefore have the same value of F. According to Lin [21], the Brillouin scattering coefficient is about 13 percent as large as the Rayleigh coefficient.

Theoretical values for the Rayleigh scattering capture fractions have been derived by several authors [2,21,33,34,35]; we will use the results of Neumann [4] as follows:

For a step-index fiber

$$F = \frac{3(NA)^2}{8\ n_1^2} \tag{4-2}$$

and for a graded-index fiber

$$F = \frac{(NA)^2}{4\ n_1^2}\ . \tag{4-3}$$

In both equations n_1 is the value of refraction on the fiber axis. We see than, that for identical NA and n_1 values the capture fractions for a graded-index fiber are smaller than the step-index fiber by a factor of 2/3.

The approach we have taken for the experimental determination of F is based on eq (1-1) where a known signal level is compared with the observed backscatter signal level. A convenient "calibrated" signal level in this case is the Fresnel reflection from a perfect fiber break. The ratio of the power reflected Φ_r to the power backscattered for an ideal cleave Φ_s is given by [27]

$$\frac{\Phi_r}{\Phi_s} = \frac{2RN}{\alpha_s cWF} \tag{4-4}$$

where W is the probe pulse width, R the Fresnel reflectivity, and the other quantities have been defined previously. This relation is independent of the total attenuation and length of the test fiber. The reflectivity is given by the relation

Table 2. Capture fractions associated with various scattering and reflection processes.

Backscatter source	Capture fraction	Remarks
Isotropic scattering	$\frac{1}{2} (\frac{NA}{n_1})^2$	single mode fiber, ref. [2]
Rayleigh scattering	$0.21 (\frac{NA}{n_1})^2$ to $0.24 (\frac{NA}{n_1})^2$	single mode fiber, ref. [47]
Rayleigh scattering	$\frac{3}{8} (\frac{NA}{n_1})^2$	multimode step index, ref. [4]
Rayleigh scattering	$\frac{1}{4} (\frac{NA}{n_1})^2$	multimode graded index, ref. [4]
Reflection from break	1	Fresnel reflection
Reflection from break end face tilt angle 4°	0.46	Step index, $\Delta = 0.01$ ref. [38]
Reflection from break end face tilt angle 4°	0.26	graded index $\Delta = 0.01$ ref. [38]
Fiber bends	$< 6 \times 10^{-4}$	Section 5 experimental data
Pressure-induced microbending	$< 5 \times 10^{-5}$	Section 5 experimental data

$$R = \frac{(n_1-1)^2}{(n_1+1)^2} \tag{4-5}$$

If we assume that the entire core is of index n_1, and the cleave is a mirror surface perpendicular to the fiber axis. We can then relate F to quantities which are observables as follows:

$$F = \frac{2(n_1-1)^2 N}{(n_1+1)^2 \alpha_s cW} \frac{\Phi_s}{\Phi_r} \tag{4-6}$$

In our experiment we measure α_s as described in section 4.2, and estimate N and n_1 according to section 4.4. The probe pulse is nearly rectangular and its width W is easily obtained from an oscilloscope trace. The ratio Φ_r/Φ_s is determined as follows: The fiber was cleaved and examined for end quality (see section 4.3.3). Since the power level Φ_r is large compared with Φ_s (typically +30 dB), it is necessary to place a carefully calibrated neutral density filter with attenuation constant K in front of the detector at the position noted in figure 2-1. The rays at this point are approximately parallel so that no corrections are necessary for the NDF attenuation, and the location of the focus on the APD is unchanged. The detector is mounted on an XYZ translator so that it is easy to check for a signal maximum. After the signal level $K\Phi_r$ from the fiber break is noted, the fiber end is immersed in an index matching fluid to suppress unwanted reflections and the backscatter signal Φ_s is observed at the same location in the fiber. If the NDF is chosen correctly the signal level at the APD will be approximately the same as in the prior measurement of Φ_r. This tends to minimize any nonlinear response effects in the APD. Since K is known, the ratio Φ_r/Φ_s is easily deduced. This information is used with eq (4-6) to determine the values of the capture fraction for six step and graded-index fibers. At least six measurements were made on each fiber in order to obtain an estimate of the statistical errors.

4.3.3 Fiber End Preparation

In order to use eq (4-6) for the determination of capture fractions, it is essential to have the fiber ends cleaved so that they are perfectly reflecting mirror surfaces. Gloge [37] has shown that, in general, the glass fiber fracture face is composed of three regions known as the mirror, the mist and the hackle zones. If properly cleaved, the surface consists entirely of a mirror zone. In addition to being smooth and flat, the end surface must be perpendicular to the fiber axis. Marcuse [38] has shown that, for end faces tilted with respect to the plane perpendicular to the fiber axis as little as two degrees, the reflectivity can change by 30 percent (parabolic index fiber, $\Delta = 0.01$). Here Δ is the relative index difference of the fiber, $\Delta = (n_1{}^2-n_2{}^2)/2n_1{}^2$. We have used the scribe-and-pull technique of Chesler and Dabby [39] in order to produce the highest quality of fiber breaks. In this method, the fiber is held between thumb and forefinger, scribed with a silicon carbide razor blade [40], and then pulled until broken. The fiber must be pulled straight without bending. Experience has shown that this method produces fractures of superior quality to those obtained from other breaking techniques [41,42].

Table 3. Capture fraction data

Fiber	Type	10^3 F Experimental	10^3 F Theory
A	Graded	3.4 ± 0.6	4.56
B	Graded	6.1 ± 1.2	6.74
C	Graded	6.6 ± 1.3	6.83
D	Graded	2.9 ± 0.6	6.49
E	Step	2.0 ± 0.4	7.11
F	Step	5.7 ± 1.1	13.9

Table 4. Optical fiber data

Fiber	Length m	NA	α_s @ 819 nm dB/km	α_s/α_T %	Φ_r/Φ_s
A	975	0.20	3.27	71	2386
B	1300	0.24	2.07	67	946
C	1089	0.24	1.64	71	1106
D	1167	0.23	3.35	91	1346
E	782	0.20	3.00	49	1950
F	1200	0.28	2.40	78	883

The fiber-end quality was determined by microscopic examination and with an He-Ne laser technique described by Reitz [43]. With the latter method, a low power laser illuminates the end of the fiber. The quality of the end break will determine the type of reflection pattern on a remote screen. A small spot indicates a mirror surface fiber end. Diffused or large spots or visible scatter from the end indicates a poor break. The locus of points described by the reflected beam on a calibration target as the fiber is rotated, determines the end-face angle (the axis of rotation is the fiber axis). This rotation is easily done with the fingers if the fiber is held in a precision bore capillary tube [14]. With care, these angles can be kept within a degree or less of being perfectly perpendicular to the fiber axis.

4.3.4 Numerical Aperture Measurements

There are a number of interpretations and definitions of the term "numerical aperture" (NA) [44]. We have chosen the far-field equilibrium radiation pattern as the appropriate physical quantity from which we determine the numerical values of NA for use in eqs (4-2) and (4-3). Figure 4-16 is an example of such a radiation pattern from fiber C. The fiber was flooded to excite all possible modes and measurements were taken at the output end (1.2 km) in order to approximate equilibrium conditions. For our purposes we will take NA = $\sin\theta$ where θ is half the vertex angle at which the output irradiance falls to 0.05 of the on-axis irradiance. In a series of comparisons for graded-index fibers [45], the NA determined in this way has been found to agree (to within about 10 percent) with the NA derived from index measurements according to the equation

$$NA = (n_1^2 - n_2^2)^{1/2} . \tag{4-7}$$

This relation is independent of the profile parameter, that is, whether the fiber is of the step or graded-index variety. The exact identification is, however, complicated by the presence of lossy high order modes and leaky modes [46,47].

4.3.5 Results

The results of the capture fraction measurements are listed in table 3. We see that experimental F values for three of the four graded-index fiber A, B, and C agree fairly well with the result calculated from eq (4-3). Fiber D, however, has a value almost a factor of two less than expected. For the step-index fibers all measured values are less than the simple theory, eq (4-2), predicts.

Fibers A and E were from the same manufacturer, as were fibers B, C, and F. Fiber D was obtained from a third manufacturer. For reference purposes some of the properties of these fibers are listed in table 4. There does not seem to be an obvious correlation of low F values with any other of the measured fiber parameters.

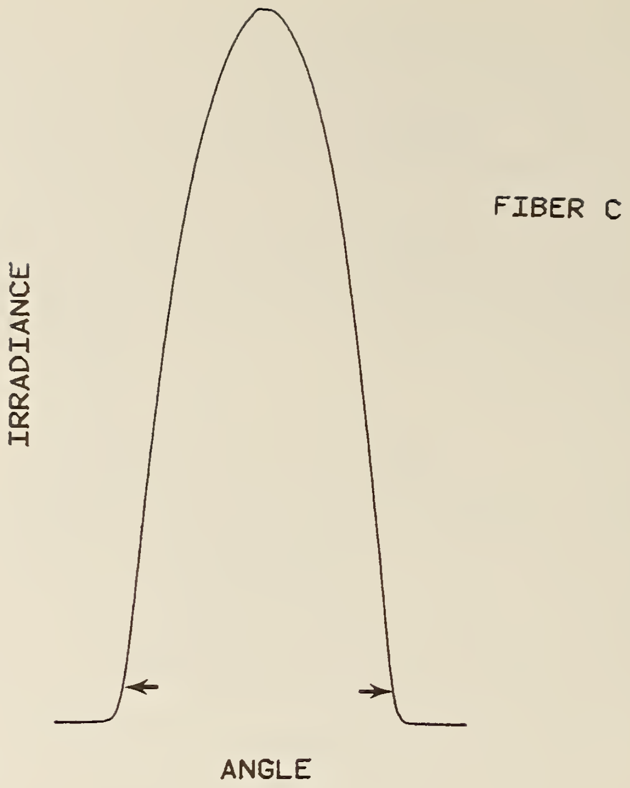

Figure 4-16. Far-field equilibrium radiation pattern which is used to determine the NA of fiber C. The angle between the 5 percent intensity points is indicated by the arrows.

4.3.6 Error Analysis

The uncertainties in the determination of F values which appear in table 2 were expressed as estimated standard errors evaluated in the following manner. The standard errors Δx_n in the independent random variables x_n and the systematic errors Δy_n in the variables y_n can be taken to contribute to the total fractional measurement standard error $\Delta F/F$ as

$$\frac{\Delta F}{F} = \left[\sum_{n=1}^{3} \left(\frac{\Delta X_n}{X_n}\right)^2 \right]^{1/2} + \sum_{n=1}^{2} \left| \frac{\Delta Y_n}{Y_n} \right| . \tag{4-8}$$

where individual measurement variables and their fractional errors are:

Power ratio Φ	0.12
Group velocity v_g	0.014
Phase index n_1	0.02
Pulse width W	0.03
Rayleigh scattering σ_s	0.10

The quantities Δx_n (for Φ, W, σ_s) represent one sigma calculated values. The systematics Δy_n (for n_1, v_g) are best estimates for the limits of error. We have then, from eq (15) $\Delta F/F = 0.19$. This number was used to calculate the tabulated uncertainties appearing in table 2.

4.3.7 Significance of Mode Strippers

Since Rayleigh scattering is approximately isotropic, it is possible for some of the rays emerging from the scattering centers on the fiber axis to be captured by the cladding. If the index of refraction of the surrounding medium is smaller than the cladding, rays may be refracted at the air-cladding interface and trapped in the backward direction. This will increase the effective capture fractions. Stone [24] has analyzed this problem and found that the one-way capture fraction F_c for a bare cladding in air is

$$F_c = \frac{1}{2} \left[1 - \frac{3}{4} \left(\frac{1}{n_1} - \frac{1}{3n_1^3}\right)\right] \tag{4-9}$$

This quantity is, rather surprisingly, independent of the cladding index of refraction and fiber diameter. The numerical value of F_c can be rather large; for example, for a core index of 1.45, the value of F_c is approximately 0.20 or a factor of approximately 100 larger than a mode-stripped fiber which has no backscattered power propagating in the cladding.

We have conducted an experiment to determine the importance of mode strippers on the backscattered signal. This was done by replacing the usual launcher described in section 2.6 by a holder that contained no index matching fluid. The backscatter signal was recorded by observation on the oscilloscope. A section of fiber close to the launching end was then placed on a mode stripper consisting of 12 cm of felt which was saturated with an oil having index greater than n_2. A weight placed on the fiber insured good optical contact with the oil. The backscatter signal was again recorded. For most of the fibers there was no perceptible change in backscatter signal. The maximum observed change represented a 12 percent drop in signal with application of the mode stripper.

These results indicate that, at least for the fibers tested here, there is a negligible amount of backscattered power propagating in the cladding. There are two possible reasons for this. The loss of the cladding is usually very high (100 dB/km) so that the radiation in the cladding is rapidly attenuated. This is particularly true for the inside vapor phase oxidation (IVPO) process where the soot is deposited on the inside of a lossy silica tube. For other manufacturing processes, for example the outside vapor phase oxidation (OVPO), the cladding may not be as lossy. Secondly, if the fiber is in contact with a jacket, coating, or other material of index greater than n_2, the rays in the cladding will escape into the surrounding medium. We conclude then, for the fibers we have tested from three different manufacturers, mode strippers do not have a significant effect on backscatter signal levels or capture fraction determinations.

4.3.8 Discussion

We see from the capture fraction results in table 2 that slightly over one half the experimental F values do not have limits of error that bracket the values predicted from simple theory. The experimental values are consistantly low. We feel that the experimental determinations of capture fractions described here represent a realistic approach to the measurement of these physical quantities and that the low values are real. This conclusion implies that there are deficiencies in the theoretical model we have used, at least as it applies to certain fiber configurations. Neumann [4] has discussed some of the approximations and physical effects which have been neglected in the derivation of eqs (4-2) and (4-3). The presence of leaky modes, mode selective attenuation, variations in the fiber material as a function of length, variations in scattering as a function of fiber radius and changes in modal energy distributions could all effect the simple theoretical predictions.

Pending independent F measurements by other investigators, we tentatively conclude that the magnitude of the capture fraction as given by eqs (4-2) and (4-3) may yield excessively large values in some fibers. The discrepancies are largest for the step-index fibers which we tested.

4.4 Length Determination and Fault Location

The OTDR also yields a quick estimate of the length of the fiber L from time-of-flight measurements. This distance is determined from observations of the time interval between Fresnel reflections at the front and far ends of the fiber according to the relation

$$L = \frac{cT}{2N} \tag{4-10}$$

where T is the time interval, c the velocity of light, and N the group index of the fiber. In order to measure time intervals with precision, it is necessary to have a source capable of emitting a fast-risetime pulse. Measurement accuracy requires a knowledge of the group index N. This information may be available from manufacturers. Experimentally, group velocities, c/N, can be fixed for a short sample of a given fiber, by means of a shuttle-pulse technique with a precision of about 0.1 percent and accuracies of approximately 0.2 percent [48]. A more convenient, though less accurate, method of estimating L from backscatter scans is by assuming a representative value of N for use in eq (17). We will now examine a possible way of accomplishing this.

The value of N can be calculated from the equation

$$N = n_1 - \lambda\frac{dn_1}{d\lambda} \tag{4-11}$$

if the wavelength dependence of the index of refraction is known. The required dispersion data for silica and a number of doped silica glasses used in optical fibers has been tabulated by Malitson [49], and Fleming [50,51]. The dispersion information may be expressed as a three-term Sellmeier relationship of the form

$$n_1^2 = 1 + \frac{a_1\lambda^2}{\lambda^2 - b_1^2} + \frac{a_2\lambda^2}{\lambda^2 - b_2^2} + \frac{a_3\lambda^2}{\lambda^2 - b_3^2} \tag{4-12}$$

where the coefficients a are related to the material oscillator strength, and b the corresponding oscillator wavelengths. We have calculated N and n_1 as a function of wavelength for three typical fiber materials using the data of Fleming and eqs (4-10) and (4-11); these appear in figures 4-17, 4-18 and 4-19. For our purposes we will assume that the 13.5 GeO_2:86.5 SiO_2 sample represents a fairly typical on-axis material for a high-bandwidth telecommunicaions fiber.

Some experimental values of N at 824 nm have been reported by Franzen [48] for a number of high-bandwidth graded-index fibers. These are reproduced in figure 4-20. It can be seen that they are consistent with the above approximation scheme.

We have been concerned above with fiber length measurements. The same considerations also apply to fault location.

5. MEASUREMENTS WITH PERTURBED FIBERS

In this section we will consider the effect that various local perturbations have on the backscatter response of an otherwise uniform and reciprocal fiber. These perturbations may be either extrinsic, for example bends, or intrinsic, for example an impurity region of high loss in the fiber. We will refer to the characteristic backscatter features as "fault signatures" which generate a change in the background Rayleigh response. It will be convenient to divide the signal returns into two categories which will be referred to as absorption-like and scatter-like fault signatures. The distinction is made clear from an examination of the computer-generated plots shown in figures 5-1 and 5-2. Scatter-like signatures are defined as those which have an increase in backscatter signal larger than the associated decrease (fig. 5-1). Likewise figure 5-2 illustrates an absorption-like signature, from which defect loss may be inferred as shown. The most general form of fault signature is a combination of both (fig. 5-3). It should be noted that there is always some absorption associated with scatter-like signatures, even though this can be rather small. Also the decrease in backscatter power on a decibel scale is twice the actual fault loss.

5.1 Absorption-like Signatures

Absorption-like fault signatures are produced by perturbations which convert the radiation in the probe pulse into heat energy, or by perturbations which scatter the radiation exclusively in the forward direction. Figure 5-4 shows the absorption-like fault signature for a fusion splice which exists at the center of the fiber. The one-way loss is approximately 0.18 dB at the splice. The cause of the other irregularities which can be seen, has not been identified. Fusion splices are known to weaken the fiber, and the backscatter technique is the only practical means of detecting the presence of these flaws once the fiber is cabled.

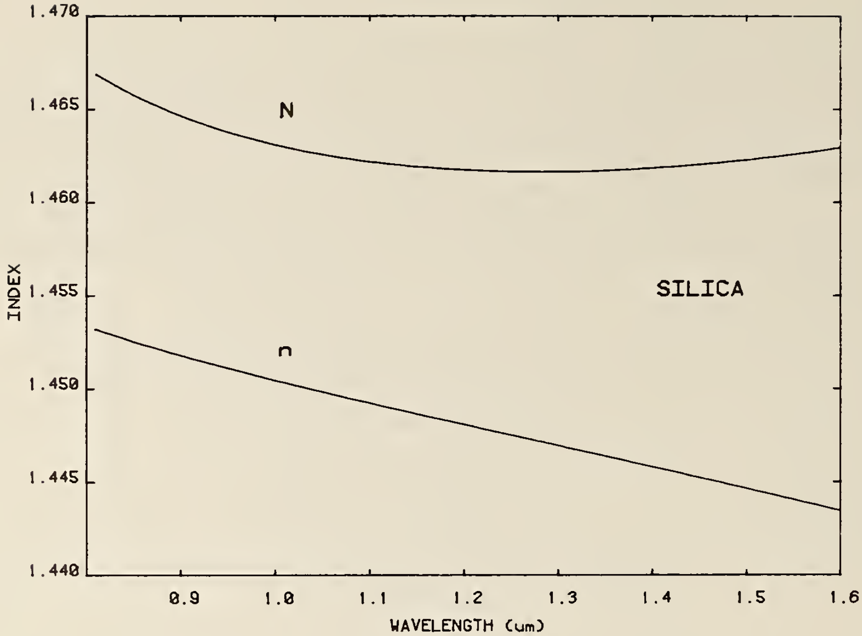

Figure 4-17. Index of refraction and group index for silica.

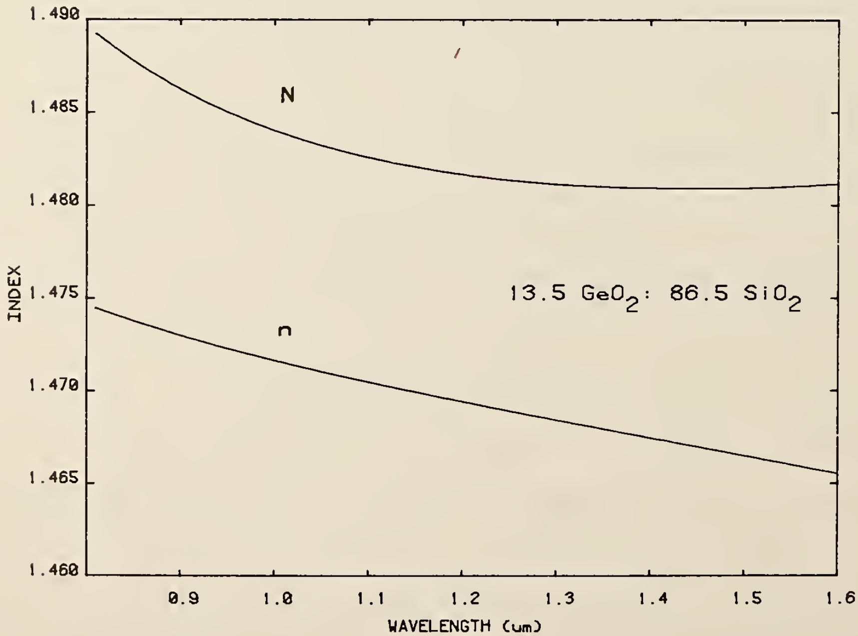

Figure 4-18. Index of refraction and group index for 13.5 GeO_2:86.5 SiO_2 glass.

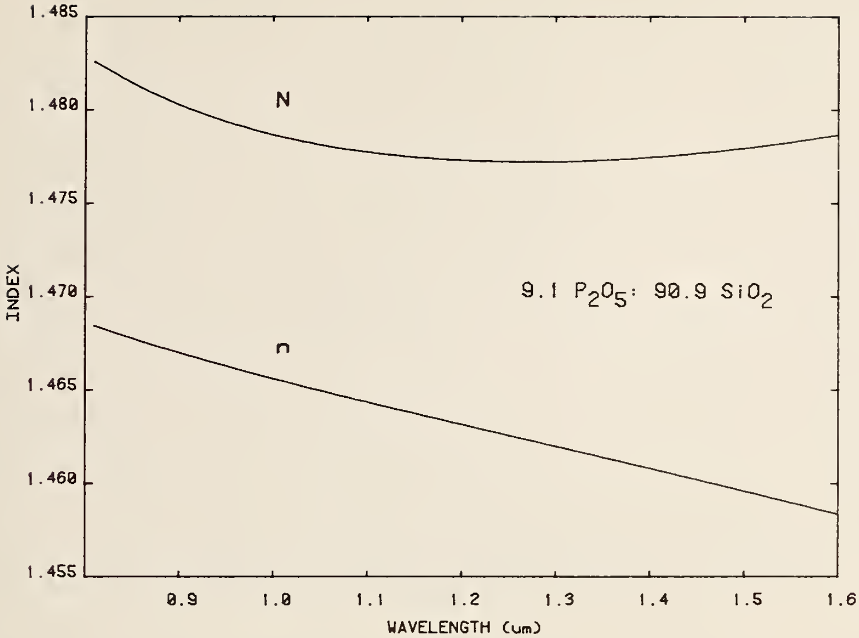

Figure 4-19. Index of refraction and group index for 9.1 P_2O_5:90.9 SiO_2 glass.

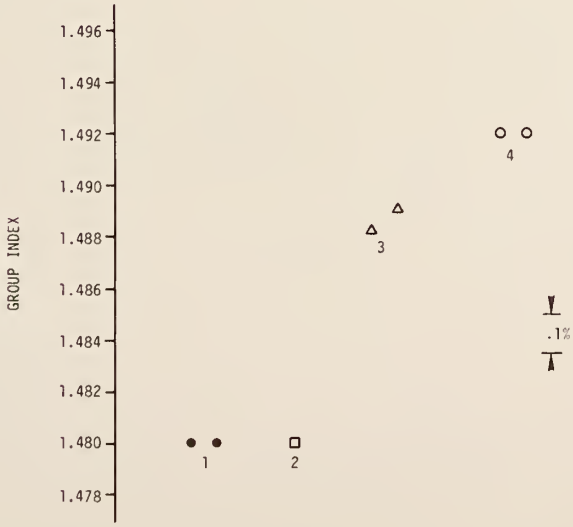

Figure 4-20. Group index measurements for five commercial fibers. Measurements on three fibers repeated to within 0.1 percent. From Franzen and Day [48].

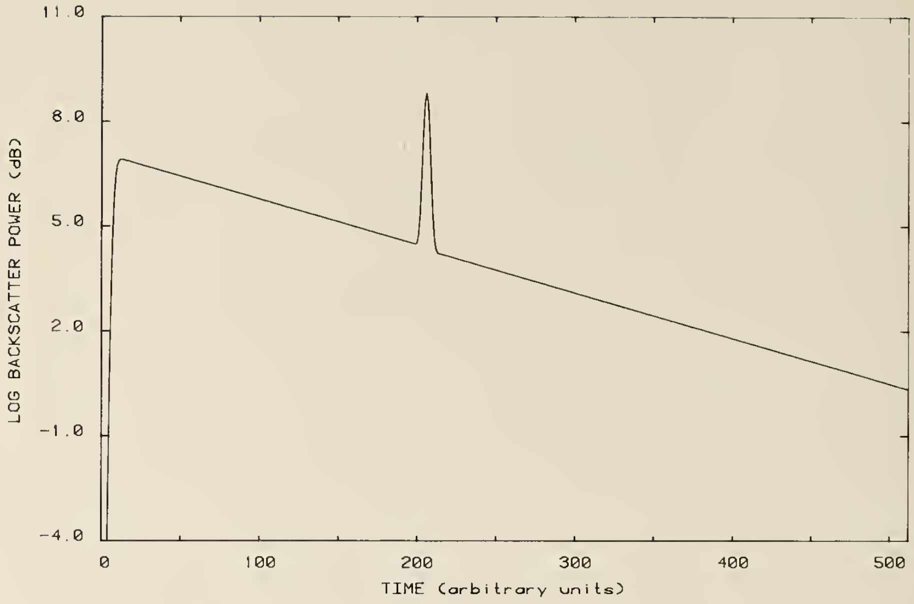

Figure 5-1. Example of a scatter-like fault signature. Gaussian probe pulse.

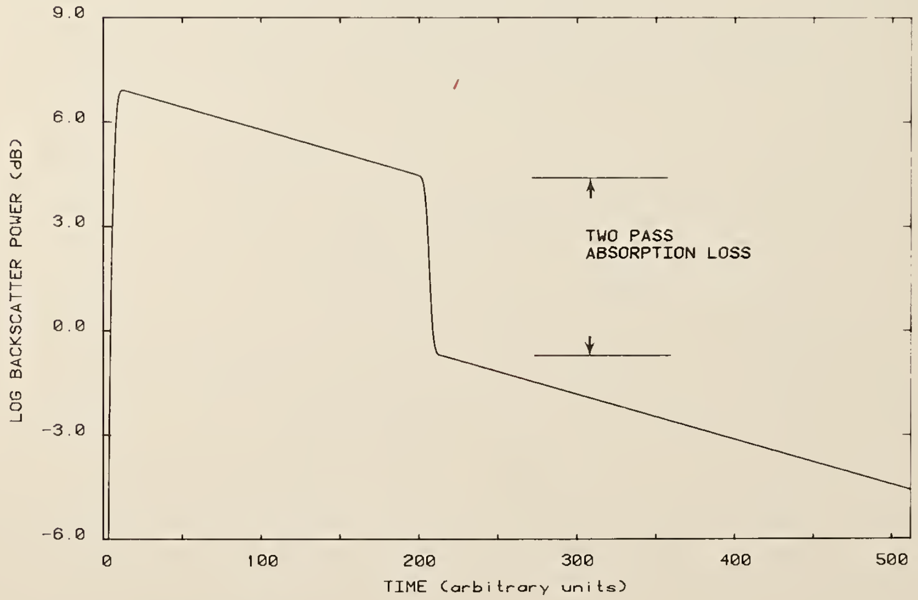

Figure 5-2. Example of an absorption-like fault signature. Gaussian probe pulse.

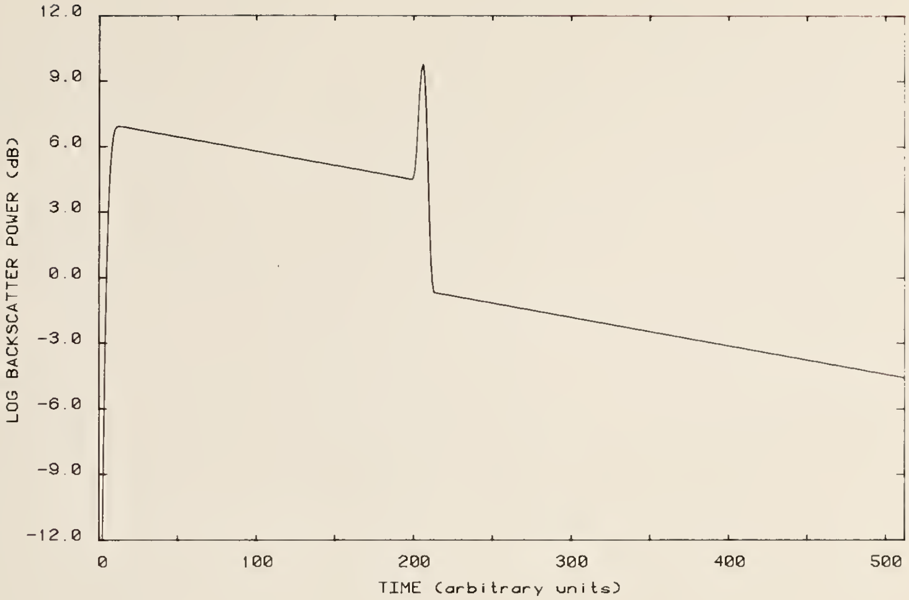

Figure 5-3. Example of a composite fault signature consisting of both scattering and absorption loss. Gaussian probe pulse.

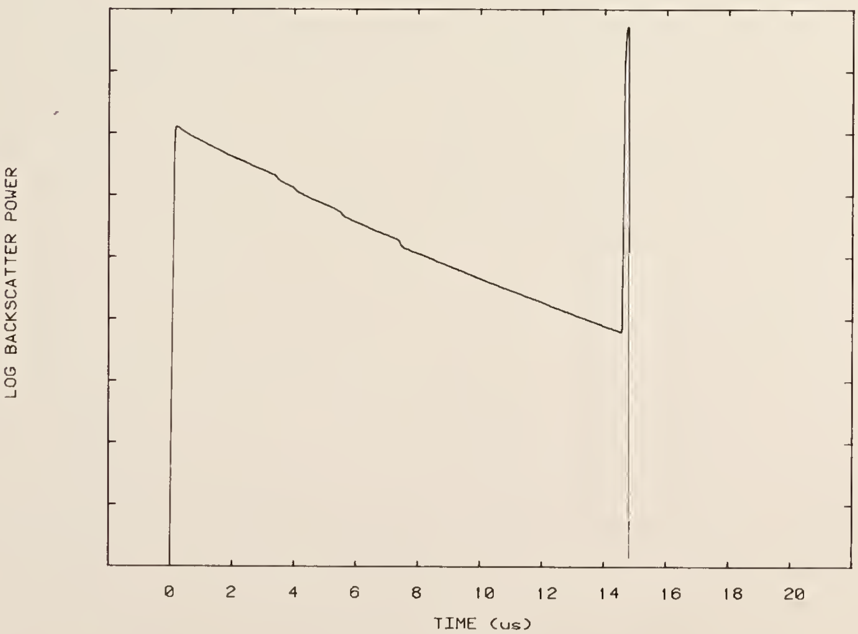

Figure 5-4. Backscatter signature for a graded-index fiber with a fusion splice at the midpoint. The three other irregularities are unidentified. Fiber J.

Microbending signatures are also absorption-like. The capture fraction associated with radiation loss due to microbending was estimated in the following experiment. We wound a 1 km graded-index fiber loosely in several layers on a felt-covered, 20 cm diameter drum. Ten plastic rods, each 6 mm in diameter, were positioned transverse to the winding. Lateral pressure was applied to the layers of fiber by pressing them against the rods using an adjustable strap concentric to the drum. The effect on the fiber is shown in figure 5-5. The lower curve represents the backscatter response with tension applied to the strap. Increased loss (about 3.1 dB total) occurs at locations where the rods were in contact with the fiber. The upper curve represents the response when the tension was removed. Some residual stress effects can still be observed. It will be noted that, in the stressed state the backscatter signal is a monotonically decreasing function of time. This implies that the capture fraction associated with the removed radiation is very small. A more quantitative estimate of the microbending capture fraction F_n may be obtained from a comparison of the two backscatter scans at t=0. From eq (1-1), the backscatter power in the stressed state differs from the corresponding power in the unstressed state only in the term $\alpha_n F_n$. Then, assuming the excess loss in figure 5-5 is a uniformly distributed radiation loss, α_n is about 7×10^{-4} m^{-1}, about the same as α_s. However, the stressed t=0 signal does not increase within an uncertainty of about one percent. This implies that $F_n < 0.01\ \alpha_s F_s/\alpha_n$, or $F_n < 5 \times 10^{-5}$. This is the basis of the estimate given in table 2.

A third example of an absorption-like signature is given by the effect of radiation from fiber bends. The magnitude of the capture fraction associated with macrobending of this sort was inferred from the following experiment. A graded-index fiber, which was loosely cabled in a plastic tube, was wound on drums of different diameters. Figure 5-6 shows the resulting signature when the input half of the 570 m cable was wrapped on a drum of 30 cm diameter and the remaining cable wrapped on a drum of 10 cm diameter. There is a small change in slope at the midpoint which implies an excess loss of about 0.9 dB/km. Most of this loss can be attributed to radiation whih is emitted as a result of the decreased bend radius. Figure 5-7 is a similar scan where the final 40 m of the cable is wound on the smaller drum, and a change in slope is also apparent. To obtain an upper limit on the macrobending capture fraction we modeled the backscattering process on a computer using the known parameters for fiber H, and assuming a value of F_n which was judged to produce a barely perceptible change in the backscatter signature. If the observed increase in radiation loss had one photon in 1700 returned in the backward direction, the signature would appear as in figure 5-8. The backscatter response in this case exhibits a signal increase at the location corresponding to the junction of the two drums. Since no such signal can be detected experimentally, we conclude that, for this fiber, $F_n < 0.0006$. This result is also given in table 2.

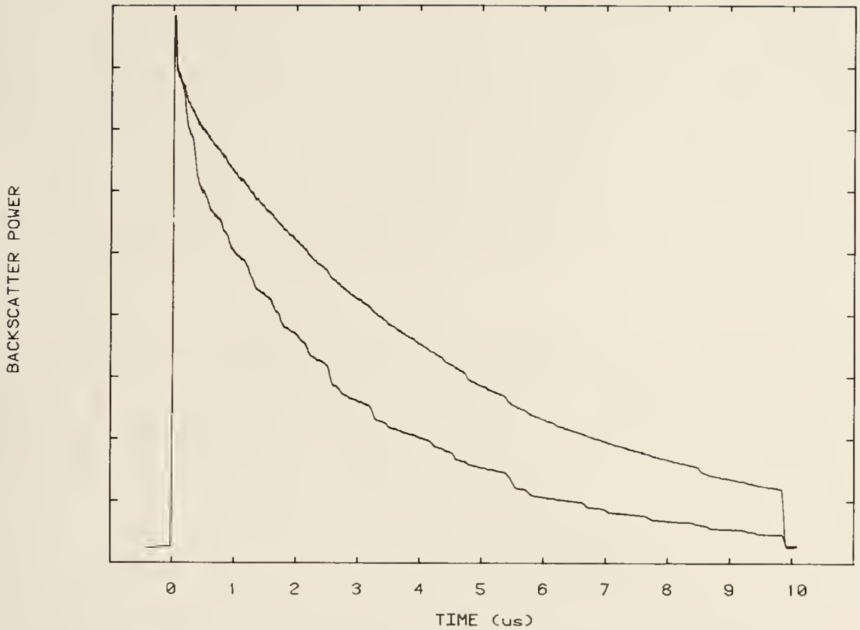

Figure 5-5. Backscatter signatures resulting from a microbending experiment (see text). Lower curve exhibits effect of pressure-induced microbending. Upper curve represents the response in the relaxed state. Fiber K.

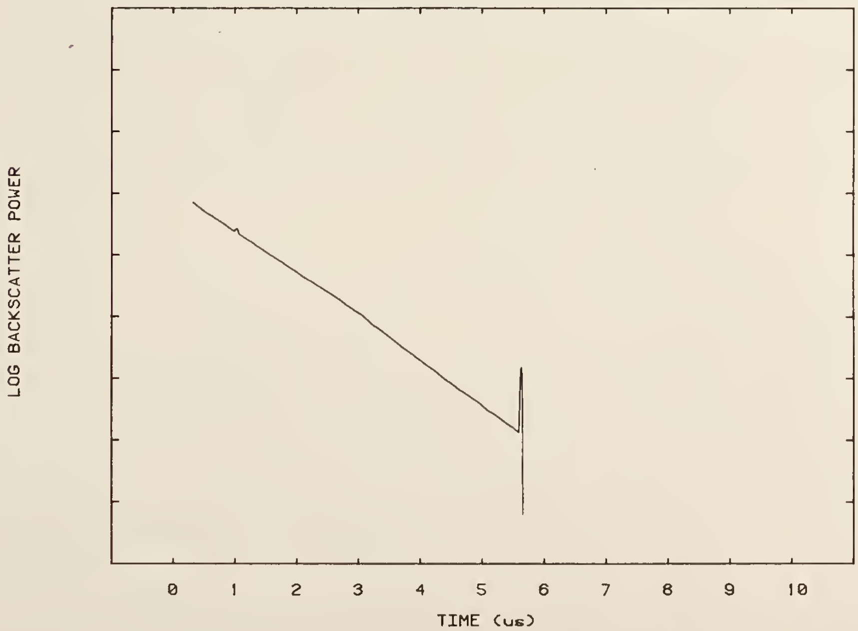

Figure 5-6. Backscatter signature for a fiber wrapped on drums of differing diameter. The input half of the fiber is wound on a drum of diameter 30 cm, the output half of the fiber is wound on a drum of 10 cm diameter. Fiber H.

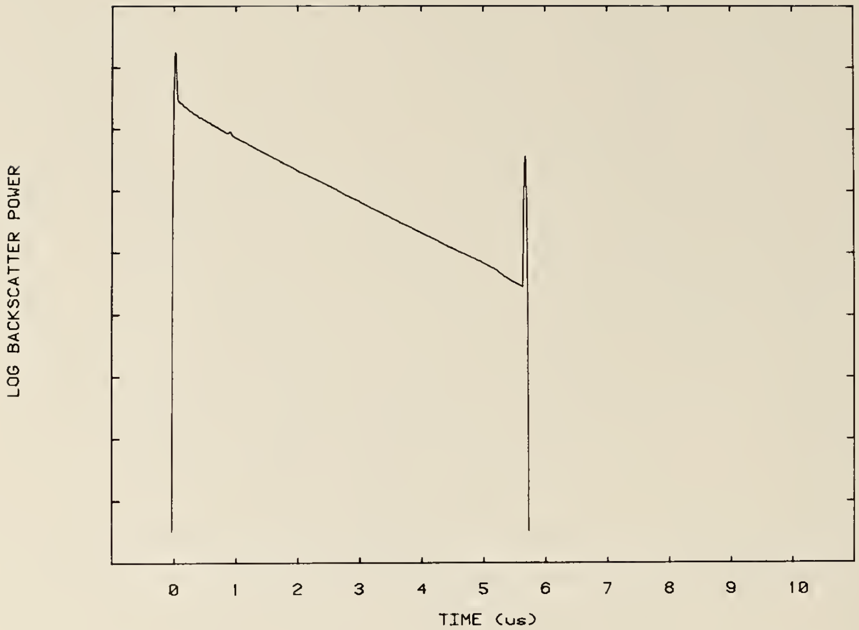

Figure 5-7. Backscatter signature under conditions similar to figure 5-6, except the final 7 percent of the fiber is on the smaller drum. Fiber H.

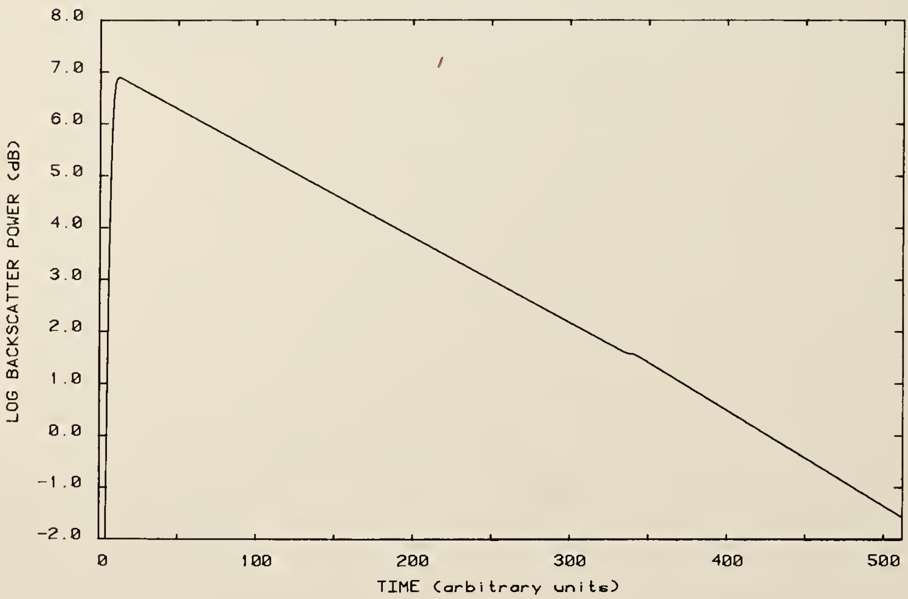

Figure 5-8. Computer simulation of radiation loss with an excess F value of 0.0006, other parameters similar to fiber H. Excess radiation loss begins at time 345.

5.2 Scatter-Like Signatures

We have seen previously, in figures 2-2 to 2-4, an example of a localized scatter-like fault signature. The scan is also reproduced in figure 5-9 on an expanded scale. The magnitude of the feature depends somewhat on the launching spot size and its location on the input face of the fiber. It is possible to observe a small decrease in the slope of the log backscatter signal following the fault. This could possibly be explained by a redistribution of probe pulse energy into less-lossy modes. The most likely explanation for the origin of the fault is an elongated bubble or dielectric filament of the type described by Rawson [52].

Figure 5-10 represents the scatter-like signature due to a commercial coupler which joins two identical step-index fibers. The signal at the junction interface is off scale. The one-way loss at the connector is about 1.4 dB. This represents a rather extreme example of a scatter-like signature.

6. COMPUTER SIMULATIONS

One of the main motivations for the experimental determination of backscatter parameters is to obtain a realistic data base for purposes of computer modeling. The actual backscatter display signatures can represent a rather complex interaction of many variables. For example, the Rayleigh as well as fault signatures will depend on absorption loss, scattering loss, capture fractions, input pulse shape, input pulse duration, wavelength, SNR, type of backscatter display (direct, logarithmic, differential logarithmic), fiber type (single mode, multimode) and the spatial distribution of any perturbations along the length of the fiber. Computer generated displays which can independently vary these parameters can greatly assist in interpreting and understanding experimental signatures. Also, we may be led to a preferred display scheme for backscatter signatures.

Some of these computer-generated signatures have appeared in this report. A much more comprehensive atlas of backscatter signatures is in preparation for a future report in this series.

7. CONCLUSIONS

We have described a laboratory OTDR in some detail, indicated its potentialities and limitations, and suggested ways in which the SNR may be improved. We have also described experimental techniques for estimating fiber Rayleigh scattering, capture fractions, and group velocities. The OTDR system was used to examine the backscatter signatures of a number of fibers and fiber perturbations. Some of the main conclusions from the experimental work may be summarized as follows:

1. Fibers from some manufacturers exhibit much smaller irregularities in background backscatter than similar type fibers from other manufacturers. These signal variations are probably due to diameter fluctuations. It is much easier to observe a perturbation or fault signature on a uniform background. Therefore, in some applications, for example

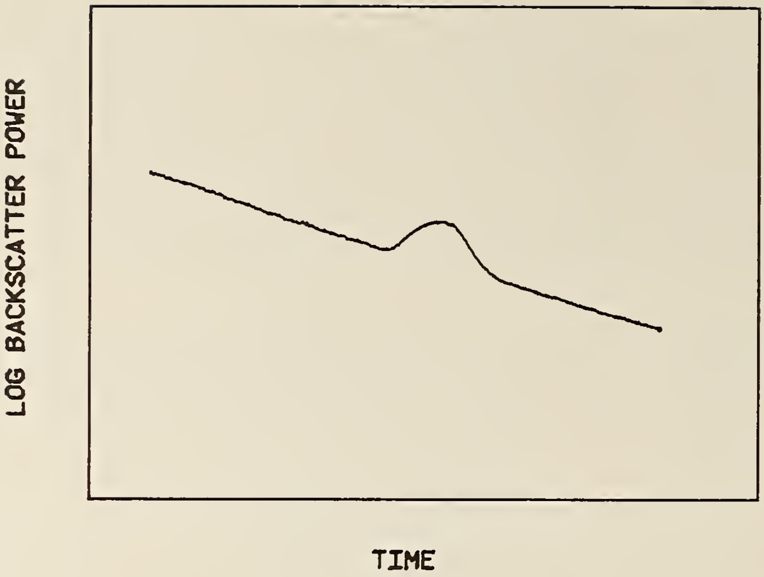

Figure 5-9. Fault signature for a bubble in a graded-index fiber. This is an expanded scale of figure 2-4. Fiber H.

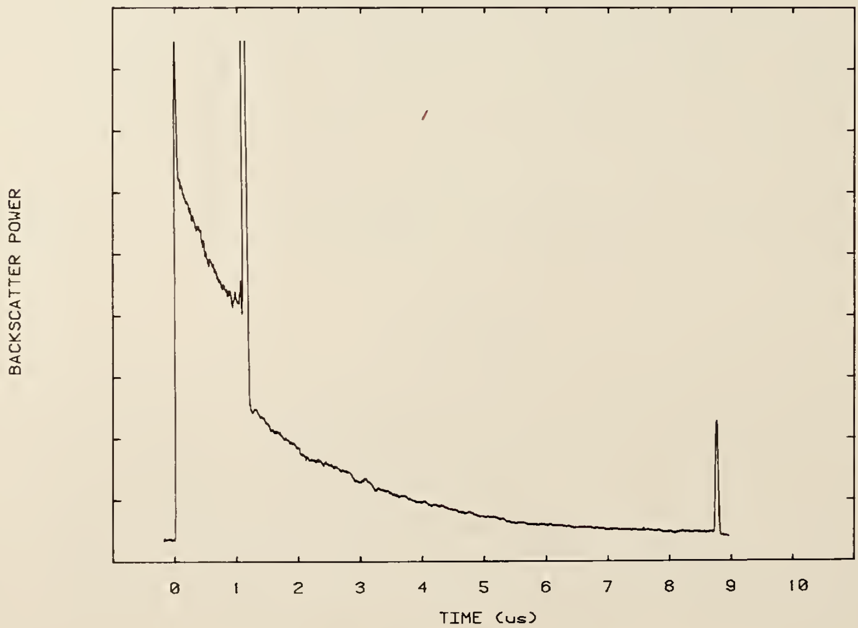

Figure 5-10. Signature for a commercial coupler. The scatter signal at 1.2 μs is off scale. Fiber E.

secure communications, it may be desirable for military agencies to specify tolerances on the oscillatory swings in the Rayleigh backscatter signature.

2. Measured capture fractions were often smaller than predicted from simple theoretical considerations. There was a large variability in the agreement of theory and experiment from fiber to fiber. The reason for this is not fully understood, but is believed to be related to the oversimplified nature of the formulae used to predict F_s values.
3. The presence of a mode stripper does not alter the backscatter signal level appreciably in the fibers we have tested. This experience may not apply to fibers manufactured with low-loss cladding materials.
4. Many types of defects and anomalies can be observed with backscatter techniques. We have classified the observed backscatter features as absorption-like and scatter-like signatures. Among the former are those due to good fusion splices, microbending, and macrobending. Among the latter are those due to some couplers, dielectric filaments, gross fractures, and breaks.
5. Upper limits have been placed on the capture fractions due to macrobending and microbending in sample fibers (table 2). The small values are due to the fact that the radiation associated with these processes is largely scattered in the forward direction.

8. REFERENCES

1. Barnoski, M. K., and Jensen, S. M., Fiber waveguides: A novel technique for investigating attenuation characteristics, Appl. Opt. 15, No. 9, pp. 2112-2115 (Sept. 1976).
2. Personik, S. D., Photon probe--an optical time domain reflectometer, Bell Syst. Tech. J. 56, No. 3, pp. 355-366 (Mar. 1977).
3. Rourke, M. D., An overview of optical time domain reflectometry, (Conference on the Physics of Fiber Optics, Chicago, IL, Apr. 28-30, 1980), to be published.
4. Neumann, E.-G., Analysis of the backscattering method for testing optical fiber cables, AEÜ, Electron. and Commun. 34, No. 4, pp. 157-160 (1980).
5. Elion, G. R., and Elion, H. A., Fiber optics in communication systems, (Marcel Dekker, Inc., New York, NY, 1978). Chapter 3 lists specifications for laser diodes from several manufacturers.
6. Certain trade names are used in this report in order to specify the experimental conditions used in obtaining the reported data. Mention of these products in no way constitutes endorsement of them. Other manufacturers may have products of equal or superior specifications.
7. Riad, S. M., Optical fiber dispersion characterization study, NASA Final Report, Contract No. NAS10-9455 (Dec. 1979).
8. Reference 5, Chapter 4 lists a number of commercially available APDs along with device specifications and much useful information.
9. Kaminow, I. R., Polarization in fibers, Laser Focus, pp. 80-84 (June 1980).
10. Born, M., and Wolf, E., Principles of optics, Second edition, (McMillan Co., New York, NY, 1964) pp. 39-40.

11. Straus, J., Few, I., and Conrad, J., Measurement of frequency dependence of Rayleigh backscattering in bidirectional optical systems, Electron. Lett. 15, pp. 306-307 (1979).

12. Costa, B., and Sordo, B., Experimental study of optical fiber attenuation by a modified backscattering technique, (Digest of technical papers presented at the Third European Conference on Optical Communication, Munich, Germany, Sept. 14-16, 1977) pp. 69-71.

13. Dakin, J. P., Gambling, W. A., Payne, D. N., and Sunak, H. R. D., Launching into glass-fiber optical waveguides, Opt. Commun. 4, No. 5, pp. 354-357 (Jan. 1972).

14. Wilmad Glass Co., Buena, NJ 08310.

15. Reference 5, p. 172.

16. Smith, R. G., Optical power handling capacity of low loss optical fibers as determined by stimulated Raman and Brillouin scattering, Appl. Opt. 11, No. 11, pp. 2489-2494 (Nov. 1972).

17. Crow, J. D., Power handling capacity of glass fiber lightguides, Appl. Opt. 13, No. 3, pp. 467-468 (Mar. 1974).

18. Danielson, B. L., An assessment of the backscatter technique as a means for estimating loss in optical waveguides, Nat. Bur. Stds. (U.S.), Tech. Note 1018, 76 p. (Feb. 1980).

19. DiVita, P., and Rossi, U., Backscattering measurements in optical fibers: Separation of power decay from imperfection contribution, Electron. Lett. 15, No. 15, pp. 467-469 (July 15, 1979).

20. Bender, A., Salisbury, G., and Akers, F., Concentric-core optical fiber, Paper THC4, Topical Meeting on Optical Fiber Communications, Technical Digest, Mar. 6-8, 1979, Washington, DC.

21. DiVita, P., and Rossi, U., The backscattering technique: Its field of applicability in fibre diagnostics and attenuation measurements, Opt. and Quantum Electron. 11, pp. 17-22 (1980).

22. Olshansky, R., Propagation in glass optical waveguides, Rev. Mod. Phys., 51, No. 2, 341-367 (Apr. 1979).

23. Olshansky, R., and Oaks, S. M., Differential mode attenuation measurements in graded-index fibers, Appl. Opt. 17, No. 11, pp. 1830-1835 (June 1978).

24. Tynes, A. R., Integrating cube scattering detector, Appl. Opt. 9, No. 12, pp. 2706-2710 (Dec. 1970).

25. Ostermayer, F. W., and Benson, W. W., Integrating sphere for measuring scattering loss in optical fiber waveguides, Appl. Opt. 13, No. 8, pp. 1900-1902 (Aug. 1974).

26. Inada, K., A new graphical method relating to optical fiber attenuation, Opt. Commun. 19, No. 3, pp. 437-439 (Dec. 1976).

27. Yoshida, K., Sentsui, S., Shii, H., and Kurona, T., Optical fiber drawing and its influence on fiber loss, Paper D9-3, 1977 International Conference on Integrated Optics and Optical Fiber Communication, July 18-20, 1977, Tokyo, Japan.

28. Blankenship, M. G., Keck, D. B., Levin, P. S., Love, W. F., Olshansky, P., Sarkar, A., Schultz, P. C., Sheth, K. D., and Siegfried, R. W., High phosphorus containing P_2O_5-GeO_2-SiO_2 optical waveguide, Post-deadline paper PD3-1, Topical Meeting on Optical Fiber Communications, Technical Digest, Mar. 6-8, 1979, Washington, DC.
29. Miller, S. E., and Chynoweth, A. G., eds., Optical Fiber Telecommunications, p. 357 (Academic Press, New York, NY, 1979).
30. Midwinter, J. E., Optical fibers for transmission, p. 159 (John Wiley & Sons, New York, NY, 1979).
31. Lin, S., and Giallorenzi, T. G., Sensitivity analysis of the Sagnac-effect optical fiber ring interferometer, Appl. Opt. 18, No. 6, pp. 915-931 (Mar. 1979).
32. Rourke, M. D., Maximum achievable crosstalk isolation in full-duplex single strand fiber-optic systems, Opt. Commun. 25, No. 1, pp. 40-42 (Apr. 1980).
33. Wells, W. H., Crosstalk in a bidirectional optical fiber, Fiber and Integrated Optics, 1, No. 3, pp. 243-287 (1978).
34. Stone, J., Measurement of Rayleigh scattering in liquids using optical fibers, Appl. Opt. 12, No. 8, pp. 1824-1827.
35. Dakin, J. P., and Gambling, W. A., Theory of scattering from the core of a multimode fiber waveguide, Opt. Commun. 10, No. 2, pp. 195-199 (Feb. 1974).
36. Neumann, E. G., Optical time domain reflectometer: Comment, Appl. Opt. 17, No. 11, p. 1675 (June 1978).
37. Gloge, D., Smith, P. W., Bisbee, D. L., and Chinnock, E. L., Optical fiber end preparation for low-loss splices, Bell Syst. Tech. J. 52, No. 9, pp. 1579-1588 (Nov. 1973).
38. Marcuse, D., Reflection losses from imperfectly broken fiber ends, Appl. Opt. 14, No. 12, pp. 3016-3020 (Dec. 1975).
39. Chesler, R. B., and Dabby, F. W., Simple testing methods give users a feel for cable parameters, Electronics, pp. 90-92 (Aug. 5, 1976).
40. Deane Carbide Products Inc., P.O. Box 118, Trevose, PA 19047.
41. Gordon, K. S., Rawson, E. G., and Nafarrate, A. B., Fiber-break testing by interferometry: A comparison of two breaking methods, Appl. Opt. 16, No. 4, pp. 818-819 (Apr. 1977).
42. Saunders, M. J., Torsion effects on fractured fiber ends, Appl. Opt. 18, No. 10, pp. 1480-1481 (May 1979).
43. Reitz, P. R., A quality check for fiber end faces, Optical Spectra, pp. 39-40 (Dec. 1979).
44. Hanson, A. G., Bloom, L. R., Day, G. W., Gallawa, R. L., Grat, E. M., and Young, M., Optical waveguide communications glossary, NTIA Special Publication NTIA-SP-79-4 (Sept. 1979).
45. Franzen, D. L., private communication.
46. Kim, E. M., and Franzen, D. L., Measurement of far-field and near-field radiation patterns from optical fibers, Nat. Bur. Stds. (U.S.), Tech. Note 1032 (to be published).
47. Brinkmeyer, E., Backscattering in single-mode fibers, Electron. Lett. 16, No. 9, pp. 329-330 (Apr. 24, 1980).

48. Franzen, D. L., and Day, G. W., Measurement of propagation constants related to material properties in high-bandwidth optical fibers, IEEE J. Quantum Electron. QE-15, No. 12, pp. 1409-1414 (Dec. 1979).

49. Malitson, I. H., Interspecimen comparison of the refractive index of fused silica, J.O.S.A. 55, No. 10, pp. 1205-1209 (Oct. 1965).

50. Fleming, J. W., Material and mode dispersion in $GeO_2 \cdot B_2O_3 \cdot SiO_2$ glasses, J. Am. Ceram. Soc., 59, No. 11-12, pp. 503-507 (Nov.-Dec. 1976).

51. Fleming, J. W., Material dispersion in lightguide glasses, Electron Lett. 14, No. 11, pp. 326-328 (May 25, 1978).

52. Rawson, E. G., Measurement of the angular distribution of light scattered from a glass fiber optical waveguide, Appl. Opt. 11, No. 11, pp. 2477-2481 (Nov. 1972).

9. ACKNOWLEDGMENT

This work was supported by the Communications Systems Center, U.S. Army Communications Command, Fort Monmouth, New Jersey 07703.

NBS-114A (REV. 9-78)

U.S. DEPT. OF COMM. BIBLIOGRAPHIC DATA SHEET	1. PUBLICATION OR REPORT NO. NBS TN-1034	2. Gov't. Accession No.	3. Recipient's Accession No.

4. TITLE AND SUBTITLE

Backscatter Measurements on Optical Fibers

5. Publication Date

February 1981

6. Performing Organization Code

7. AUTHOR(S)

B.L. Danielson

8. Performing Organ. Report No.

9. PERFORMING ORGANIZATION NAME AND ADDRESS

NATIONAL BUREAU OF STANDARDS
DEPARTMENT OF COMMERCE
WASHINGTON, DC 20234

10. Project/Task/Work Unit No.

11. Contract/Grant No.

12. SPONSORING ORGANIZATION NAME AND COMPLETE ADDRESS *(Street, City, State, ZIP)*

Communications Systems Center
U.S. Army Communications Command
Fort Monmouth, New Jersey 07703

13. Type of Report & Period Covered

14. Sponsoring Agency Code

15. SUPPLEMENTARY NOTES

☐ Document describes a computer program; SF-185, FIPS Software Summary, is attached.

16. ABSTRACT *(A 200-word or less factual summary of most significant information. If document includes a significant bibliography or literature survey, mention it here.)*

An optical time domain reflectometer (OTDR) and its components are described in detail. The system performance for this device is examined. Experimental methods are described for the measurement of several parameters of interest in the characterization of optical fibers using the OTDR. These parameters include scattering loss and capture fractions for unperturbed fibers. Experimental capture-fraction values are reported for several step and graded-index fibers and these results are compared with theoretical predictions. Rayleigh backscatter signatures are also presented for several fibers from different manufacturers. Fault signatures are shown for some intrinsic and extrinsic fiber perturbations.

17. KEY WORDS *(six to twelve entries; alphabetical order; capitalize only the first letter of the first key word unless a proper name; separated by semicolons)*

Backscattering; capture fractions; fiber scattering; optical time domain reflectometry; Rayleigh scattering.

18. AVAILABILITY	19. SECURITY CLASS (THIS REPORT)	21. NO. OF PRINTED PAGES
[XX] Unlimited	UNCLASSIFIED	52
☐ For Official Distribution. Do Not Release to NTIS	**20. SECURITY CLASS (THIS PAGE)**	**22. Price**
[XX] Order From Sup. of Doc., U.S. Government Printing Office, Washington, DC 20402	UNCLASSIFIED	$3.25
☐ Order From National Technical Information Service (NTIS), Springfield, VA. 22161		

NBS TECHNICAL PUBLICATIONS

PERIODICALS

JOURNAL OF RESEARCH—The Journal of Research of the National Bureau of Standards reports NBS research and development in those disciplines of the physical and engineering sciences in which the Bureau is active. These include physics, chemistry, engineering, mathematics, and computer sciences. Papers cover a broad range of subjects, with major emphasis on measurement methodology and the basic technology underlying standardization. Also included from time to time are survey articles on topics closely related to the Bureau's technical and scientific programs. As a special service to subscribers each issue contains complete citations to all recent Bureau publications in both NBS and non-NBS media. Issued six times a year. Annual subscription: domestic $13; foreign $16.25. Single copy, $3 domestic; $3.75 foreign.

NOTE: The Journal was formerly published in two sections: Section A "Physics and Chemistry" and Section B "Mathematical Sciences."

DIMENSIONS/NBS—This monthly magazine is published to inform scientists, engineers, business and industry leaders, teachers, students, and consumers of the latest advances in science and technology, with primary emphasis on work at NBS. The magazine highlights and reviews such issues as energy research, fire protection, building technology, metric conversion, pollution abatement, health and safety, and consumer product performance. In addition, it reports the results of Bureau programs in measurement standards and techniques, properties of matter and materials, engineering standards and services, instrumentation, and automatic data processing. Annual subscription: domestic $11; foreign $13.75.

NONPERIODICALS

Monographs—Major contributions to the technical literature on various subjects related to the Bureau's scientific and technical activities.

Handbooks—Recommended codes of engineering and industrial practice (including safety codes) developed in cooperation with interested industries, professional organizations, and regulatory bodies.

Special Publications—Include proceedings of conferences sponsored by NBS, NBS annual reports, and other special publications appropriate to this grouping such as wall charts, pocket cards, and bibliographies.

Applied Mathematics Series—Mathematical tables, manuals, and studies of special interest to physicists, engineers, chemists, biologists, mathematicians, computer programmers, and others engaged in scientific and technical work.

National Standard Reference Data Series—Provides quantitative data on the physical and chemical properties of materials, compiled from the world's literature and critically evaluated. Developed under a worldwide program coordinated by NBS under the authority of the National Standard Data Act (Public Law 90-396).

NOTE: The principal publication outlet for the foregoing data is the Journal of Physical and Chemical Reference Data (JPCRD) published quarterly for NBS by the American Chemical Society (ACS) and the American Institute of Physics (AIP). Subscriptions, reprints, and supplements available from ACS, 1155 Sixteenth St., NW, Washington, DC 20056.

Building Science Series—Disseminates technical information developed at the Bureau on building materials, components, systems, and whole structures. The series presents research results, test methods, and performance criteria related to the structural and environmental functions and the durability and safety characteristics of building elements and systems.

Technical Notes—Studies or reports which are complete in themselves but restrictive in their treatment of a subject. Analogous to monographs but not so comprehensive in scope or definitive in treatment of the subject area. Often serve as a vehicle for final reports of work performed at NBS under the sponsorship of other government agencies.

Voluntary Product Standards—Developed under procedures published by the Department of Commerce in Part 10, Title 15, of the Code of Federal Regulations. The standards establish nationally recognized requirements for products, and provide all concerned interests with a basis for common understanding of the characteristics of the products. NBS administers this program as a supplement to the activities of the private sector standardizing organizations.

Consumer Information Series—Practical information, based on NBS research and experience, covering areas of interest to the consumer. Easily understandable language and illustrations provide useful background knowledge for shopping in today's technological marketplace.

Order the **above** *NBS publications from: Superintendent of Documents, Government Printing Office, Washington, DC 20402.*

Order the **following** *NBS publications—FIPS and NBSIR's—from the National Technical Information Services, Springfield, VA 22161.*

Federal Information Processing Standards Publications (FIPS PUB)—Publications in this series collectively constitute the Federal Information Processing Standards Register. The Register serves as the official source of information in the Federal Government regarding standards issued by NBS pursuant to the Federal Property and Administrative Services Act of 1949 as amended, Public Law 89-306 (79 Stat. 1127), and as implemented by Executive Order 11717 (38 FR 12315, dated May 11, 1973) and Part 6 of Title 15 CFR (Code of Federal Regulations).

NBS Interagency Reports (NBSIR)—A special series of interim or final reports on work performed by NBS for outside sponsors (both government and non-government). In general, initial distribution is handled by the sponsor; public distribution is by the National Technical Information Services, Springfield, VA 22161, in paper copy or microfiche form.

U.S. DEPARTMENT OF COMMERCE
National Bureau of Standards
Washington, D.C. 20234

OFFICIAL BUSINESS

Penalty for Private Use, $300

POSTAGE AND FEES PAID
U.S. DEPARTMENT OF COMMERCE
COM-215

U.S.MAIL

SPECIAL FOURTH-CLASS RATE
BOOK